TR-O-0071

41

GaAs(111)Aパターン基板上でのGaAs/AlGaAs多層膜の分子線エピタクシー中のファセット成長

武部　敏彦

1994. 3. 31

ATR光電波通信研究所

ATR Technical Report

報告題名 ： GaAs(111)Aパターン基板上でのGaAs/AlGaAs多層膜の分子線エピタクシー中のファセット成長*

報告者 ： 武部 敏彦

所属 ： ATR光電波通信研究所 通信デバイス研究室

報告内容概要 ：

【1】研究の動機

GaAs(001)パターン基板上のGaAs、AlGaAs、InGaAsの成長、及びそれに基づいたデバイス応用に関しては数多くの報告がある。特に、[$\bar{1}$10]と[110]方向のストライプパターンを有する(001)基板上での分子線エピタクシー(MBE)中のファセット成長はよく研究されている。一方この10年間に、良好な表面モルフォロジーを示すGaAs、AlGaAs層が($\bar{1}\bar{1}\bar{1}$)Bと(110)基板上に成長できるようになったが、(111)A基板上の良質なGaAs、AlGaAs層の成長は依然として研究の対象であった。しかし、最近漸く我々のグループで良質なGaAs、AlGaAs層、及びGaAs/AlGaAs単一量子井戸のMBEによる成長に成功した。また、これを基に、選択エッチングにより半絶縁性(111)A基板上に形成した正三角形の台状パターンにSiドープGaAsを成長することにより、Siの両性不純物としての性質と(111)A面の3回対称性を利用して、横方向p-n接合で囲まれたキャリア閉じ込め構造の試作に成功した。

そのような構造が適切にキャリア閉じ込め機能を発揮するには、均一なn型側壁層の成長と横方向p-n接合界面での急峻な伝導型の遷移が基本的に必要である。従って、デバイス応用のみならず基礎的な材料研究の観点からも、正三角形パターン上での成長過程を理解し制御することは極めて重要で興味深いことである。本報告は、GaAs(111)A基板上の正三角形パターン上にMBEでGaAs/AlGaAs多層膜を成長する間に生じるファセットを初めて系統的に論じたものである。側壁傾

斜角によるファセット発生の変化あるいは制御について詳細に論ずる。

【2】研究の成果

GaAs(111)A基板上に$HF+H_2O_2+H_2O$エッチング液※による選択エッチングで(001)面関連、(110)面関連、及び(201)面関連の側壁を有する3種類の正三角形台状パターンを形成した。これらをそれぞれ(001)三角形、(110)三角形、及び(201)三角形と名付ける。この上に、MBEでGaAs/AlGaAs多層膜を成長させ、成長中に生じるファセットを側壁傾斜角θと関連付けて調べた。結果は以下の様にまとめられる。

1. (001)三角形では、$(\bar{1}\bar{1}3)$A、(001)、及び(114)Aファセットが、(110)三角形では、$(11\bar{1})$B、(110)、及び(113)Aファセットが、(201)三角形では、$(\bar{1}01)$、$(\bar{2}38)$、$(\bar{1}25)$、及び(159)ファセットが、θに応じて側壁上に発生し、元の三角形パターンを変形させた。

2. この中で、(114)A、(110)、及び(159)ファセットは広いθ範囲にわたって存在し、従って(111)Aパターン基板上で平坦で均一な側壁層を形成するのに重要な要素である。

3. 一方、(110)及び(NNM)A (N=2, 3, -- ; M≦N-1)ファセットが(001)及び(201)三角形のコーナー上に発生した。これらも元の三角形パターンを変形させ、しかもこの上に成長したSiドープGaAsが(111)A面同様p型伝導を示すので、キャリア閉じ込め上も重要な要素である。(110)三角形のコーナー上にはファセットは生じなかった。

4. 側壁上にもコーナー上にもファセットを生じさせず、元の三角形パターンを維持しながら成長させるには、(001)三角形では33°≧θ≧29°、(110)三角形では30°≧θ≧16°、(201)三角形では33°≧θ≧26°にθを制御する必要がある。

5. 上記θを満たす3種の三角形の内、SiドープGaAsの成長で良好な横方向p-n接合、従って、キャリア閉じ込め構造が形成できるのは(001)及び(201)三角形で、(110)三角形ではキャリア閉じ込め効果を示さなかった。

6. 基板面が(111)Aから微傾斜すると、三角形パターン上で非対称な成長が進行し、基板面上の成長層が平坦でなくなり、4.のθ制御基準が破られてしまう。

7. (111)A面上でのMBE成長時に見られるピラミッド状のミクロ構造や、(111)A微傾斜面上でのMBE成長時に見られるステップ構造は(110)関連のファセットで構成されており、3.に記されている三角形コーナーでの(110)及び(NNM)Aファセットの選択的発生と深く関係している。

以上

* 本報告は、本文中ではPaper Iと名付けられている。

※ ATR Technical Report 「GaAs選択エッチング用$HF+H_2O_2+H_2O$混合液の基本特性」。

目次

Facet Generation During Molecular Beam Epitaxy of GaAs/AlGaAs Multilayers on GaAs (111)A Patterned Substrates

-Abstract-

Extra facet generation during molecular beam epitaxy of GaAs/AlGaAs multilayers on exact (111)A GaAs substrates patterned with ridge-type triangles with (001)-related, (110)-related, and (201)-related sidewalls, designated as "(001) triangle", "(110) triangle", and "(201) triangle", respectively, has been investigated for the first time. Extra $(\bar{1}\bar{1}3)$A, (001), and (114)A facets have been confirmed to generate on the (001)-related sidewalls, extra $(11\bar{1})$B, (110), and (113)A facets on the (110)-related sidewalls, and extra $(\bar{1}01)$, $(\bar{2}38)$, $(\bar{1}25)$, and (159) facets on the (201)-related sidewalls, depending on the intersection angle θ of the sidewall and the substrate plane. Of these, the (114)A, (110), and (159) facets were important because they persisted over a wide range of θ and, therefore, played a detrimental role in forming flat and uniform sidewall layers on the (111)A patterned substrates. The (110) and (NNM)A (N=2, 3, --; M≦N-1) facets developed on the corners of the (001) and (201) triangles, while no extra facets developed on the corners of the (110) triangles. It has been made clear that flat and uniform layers maintaining the initial as-etched triangle patterns can be grown without generating any extra facets on the sidewalls or corners for the (001) triangles with $33\,^{\circ} \geqq \theta \geqq 29\,^{\circ}$, the (110) triangles with $30\,^{\circ} \geqq \theta \geqq 16\,^{\circ}$, and the (201) triangles with $33\,^{\circ} \geqq \theta \geqq 26\,^{\circ}$. Asymmetric growth proceeded on the triangle patterns and violated the above criteria when misoriented (111)A substrates were used. Generation of pyramidal microstructures on exact (111)A substrates and step structures on misoriented (111)A substrates during MBE

growth, both composed of equivalent (110)-related facets, has been suggested to be closely related to the preferential generation of the (110) and (NNM)A facets found in the present study.

Key words : gallium arsenide, aluminum gallium arsenide, patterned substrate, molecular beam epitaxy, crystal facet.

1. Introduction

There have been many reports published on the growth of GaAs, AlGaAs, and InGaAs on GaAs (001) patterned substrates and device applications based on it. In particular, generation of extra facets during molecular beam epitaxy (MBE) on (001) substrates patterned with stripes running in the [$\bar{1}$10] and [110] directions has been well studied [1-20]. During the past decade, GaAs and AlGaAs layers with good surface morphology have come to be successfully grown on ($\bar{1}\bar{1}\bar{1}$)B substrates [21-31] and (110) substrates [32-40]. However, the growth of high-quality GaAs and AlGaAs on GaAs (111)A substrates is itself still a subject of research and only a few papers have been published on the growth on (111)A surfaces [31, 41-44], except for ours shown below.

We have systematically investigated crystal growth and impurity doping characteristics on (111)A substrates using MBE technique [45-60]. It has been found in the course of the research that the technological accumulation on (001) substrates and epitaxial growth on them is not directly applicable to (111)A substrates because of the difference in the surface chemical and electronic properties resulting from the different surface atomic configuration. We have recently succeeded in the MBE growth of GaAs layers with an excellent surface morphology by developing novel pre-growth chemical and thermal surface treatments [56], and in the fabrication of GaAs/AlGaAs single quantum wells with a steep and smooth heterointerface [48], on exact (111)A substrates. In addition, we have found for the first time that hexagonal AlAs grows on the exact GaAs (111)A surface [61], which we think has opened a new phase of crystallography and crystal growth on surfaces other than (001). On misoriented (111)A substrates, we have succeeded in fabricating p-n junctions by growing Si-doped GaAs alone by taking advantage of the amphoteric Si doping characteristics that depend on the growth conditions [52]. We also have established extensive control of the slope of the sidewalls through selective chemical etching of the (111)A surface using newly developed $HF+H_2O_2+H_2O$ mixtures for preparing patterned substrates [60]. On the basis of these

achievements, we have successfully created a novel carrier confinement structure with a p-type (111)A triangular region surrounded by three equivalent (113)A n-type sidewalls, that is, a lateral p-n junction, by MBE growth of Si-doped GaAs on selectively etched semi-insulating GaAs (111)A substrates [49-51, 57]. The idea for the structure is based on the acceptor nature of Si dopants on the (111)A surface in contrast to the donor-nature on (113)A surfaces and the three-fold rotational symmetry of the (111)A surface. We have also successfully fabricated "lateral p-n subband junctions" that combined vertical quantum confinements with lateral p-n junctions on stripes with the (113)A sidewall and observed "lateral" intersubband recombination emissions and tunneling currents under foward bias [58].

Uniform n-type sidewalls and a steep conduction type transition at the lateral p-n junction are basically required for the successful fabrication of such devices. It is very interesting and important to understand and control the fundamental growth process on triangle patterns not only from the point of view of device application but also from the point of view of basic material research. This paper, designated as Paper I, reports extra facet generation on the sidewalls of ridge-type triangles on exact (111)A substrates during MBE growth of GaAs/$Al_{0.3}Ga_{0.7}As$ multilayers for the first time, and discusses facet generation control in connection with the slope of the sidewall to the (111)A substrate plane. Effects of substrate misorientation on the growth process on triangle patterns are also discussed.

2. Experiment

Considering the three-fold rotational symmetry of the (111)A surface, ridge-type equilateral triangle patterns are fundamental units. Three kinds of ridge-type equilateral triangles with heights of 5 - 7 μm whose three crystallographically equivalent sidewalls are composed of (001)-related, (110)-related, and (012)-related surfaces were formed on (111)A substrates using photolithography and selective etching techniques. For simplicity, they are briefly designated as "(001)

triangle", "(110) triangle", and "(201) triangle", respectively. These triangles are schematically shown with respect to the atomic configuration of the (111)A surface in Figure 1. The (021) triangle is a mirror image of the (201) triangle with respect to the $(\bar{1}10)$ plane and has sidewall orientations equivalent to the (201) triangle. The intersection angle θ of the sidewall and the (111)A substrate plane was varied in the range from 84° to 11° for the (001) triangle, from 74° to 11° for the (110) triangle, and from 72° to 12° for the (201) triangle, respectively, using H_2O_2-excess $HF+H_2O_2+H_2O$ mixtures of various compositions [60]. These θ ranges include various low- and high-index planes for the sidewalls. The (111)A patterned substrates were then chemically etched in an $NH_4OH:H_2O_2:H_2O=2:1:96$ (volume ratio) mixture and thermally treated at 700 °C under an As_4 pressure of 4.0×10^{-5} Torr. Finally, five pairs of undoped 0.2 μm thick GaAs / 0.2 μm thick $Al_{0.3}Ga_{0.7}As$ layers and an undoped 0.3 μm thick GaAs cap were successively grown by MBE on the (111)A patterned substrates at a substrate temperature of 620 °C, an As_4 pressure of 3.3×10^{-5} Torr, a V/III flux ratio of 7.4 for GaAs and 6.2 for AlGaAs, and a substrate rotation speed of 60 rpm. The growth rate was 0.77 μm/h for GaAs and 1.10 μm/h for AlGaAs, corresponding to 0.66 and 0.94 monolayers/sec, respectively. The AlGaAs layers were used as "markers" in order to observe how the growth proceeded. The layers grown on the triangle patterns have been closely examined by scanning electron microscopy (SEM) at an acceleration voltage of 10 kV and a probe current of 1 nA as shown in Figure 1. For a cross-sectional observation, the $(\bar{1}10)$ cleaved surface was stain-etched in an $HF:H_2O_2:H_2O=1:1:10$ (volume ratio) mixture to clearly reveal the GaAs/AlGaAs interfaces. No variations in the as-etched sidewall profile, growth rate, and after-growth surface morphology were confirmed across the whole sample (20×25 mm^2) for any of the samples investigated.

3. Results and Discussion

Although the epilayer - substrate interface was not clearly observed since the first layer grown was GaAs, a definite interface maintaining the initial etching

profile was confirmed on Si-doped GaAs single layers grown under similar conditions and stain-etched more deeply.

1. (001) triangle

Figure 2 shows ($\bar{1}10$) cross-sectional views of the as-etched profiles of the (001)-related sidewalls with various values of θ. The surface index (lmn) corresponding to each value of θ is also shown (within $\pm 2°$) with $l, m, n \leqq 9$. As demonstrated in [60], the flatness and sharp intersection with the substrate plane of these sidewalls should be noted. Figure 3 shows ($\bar{1}10$) cross-sectional views of the corresponding grown layers. The brighter layers correspond to GaAs and the darker layers to AlGaAs. Local thickness variation took place in both the GaAs and AlGaAs layers but predominantly occurred in the GaAs layers, hence, the AlGaAs layers really acted as markers. Generation of extra facets on the sidewalls is described as follows:

(a) For $\theta > 80°$, extra ($\bar{1}\bar{1}3$)A, (001), and (114)A facets with facet angles $\theta_f = 80°$, 55°, and 33° to the (111)A plane, respectively, were identified.

(b)-(d) For $80° \geqq \theta > 55°$, the ($\bar{1}\bar{1}3$)A facet disappeared and the (001) and (114)A facets remained.

(e)-(h) For $55° \geqq \theta > 33°$, only the (114)A facet continued to be present. Moreover, the (114)A facet developed more towards the sidewall as θ approached 33°, θ_f for this facet, as demonstrated in (g) and (h). This may be caused by enhancement of the lateral growth due to the increase in the terrace width of microsteps formed on the as-etched sidewall.

(i)-(j) For $33° \geqq \theta \geqq 16°$, the (114)A facet finally disappeared and no extra facets were generated, leading to a flat and uniform sidewall maintaining the initial as-etched profile. Thus, the (114)A facet is the most important element to be controlled in producing a flat and uniform sidewall. The general rule of facet generation with respect to θ is, therefore, that a facet present for a large θ vanishes once θ decreases below θ_f of the facet.

(k) For $\theta < 16°$, steps with $\theta_f = 16°$ appeared near the sidewall - substrate plane boundary.

Figure 4 shows bird's eye views of the growth behavior of the (114)A facet (indicated by an arrow) with respect to θ. The characteristic surface morphology of the (114)A facet [4, 6, 14] is clearly observed and does not change with θ. The development of the (114)A facet towards the sidewall with decreasing θ is also clearly observed. The surface of the layer grown on the sidewall is smooth independent of θ.

Figure 5 shows top views of the as-etched profiles of the corners of the (001) triangles with various values of θ. Figure 6 shows top views of the corners of the (001) triangles after growth. Generation of extra facets on the corners is described as follows.:

(a) For $\theta > 80°$, no definite extra facets were seen on the corner.

(b)-(e) For $80° \geqq \theta \geqq 54°$, an extra (110) facet started to develop and increasingly grew towards the bottom of the corner with decreasing θ.

(f)-(i) Once θ decreased below 54°, however, the (110) facet decomposed into two parts which have orientations more associated with the two intersecting sidewalls. For $54° > \theta > 29°$, No extra facets were generated on the corner and a definite intersection line existed there.

(j)-(l) Below $\theta = 29°$, (110)-related facets, designated in terms of (NNM)A (N=2, 3, --; $M \geqq N/2$), appeared.

The identification of the (110) and (NNM)A facets was made on the basis of their orientations and of the values of θ_f evaluated as follows. The angle, θ_c, of the intersection line to the (111)A substrate plane can be evaluated from the experimentally determined value of θ using the simple relation $\theta_c = \tan^{-1}(\tan\theta/2)$. The value of $\theta_c = 35°$, corresponding to θ_f of the (110) facet, corresponds to $\theta = 54°$. This calculation coincides well with the experimental result that the facet appearing on the corner for $\theta \geqq 54°$ disappeared for $\theta \leqq 52°$ and confirms that the facet in question is really (110)-oriented. The value of $\theta = 29°$, corresponding to the existence boundary of the (NNM)A facets gives the value of $\theta_c = 16°$. This value corresponds to θ_f of the (221)A plane. The (NNM)A facets

shown in Figures 6(j), (k), (l) correspond to (774)A, (885)A, and (554)A, respectively.

It has been reported that the (110) and (NNM)A planes show p-type conduction by Si-doping as does the (111)A plane [32-34, 62]. In fact, the (110) triangles, described in the subsequent section, did not show any carrier confinement functions [52], which means that the (NNM)A sidewalls are p-type. Therefore, the (110) and (NNM)A facets that develop on the corner can act as carrier leakage paths and should be suppressed for a firm carrier confinement. We confirmed that facet generation cannot be controlled by the V/III ratio (7.5-5.8) or cannot be well suppressed by the lowering of the growth temperature (down to 580 °C). The lowering of the growth temperature makes it difficult to grow good p-type layers on (111)A substrates by Si-doping. Consequently, the control of θ is the only way to achieve successful suppression of facet generation.

Table 1 summarizes the facet generation behavior for the (001) triangle. In order to obtain flat and uniform layers on the sidewall maintaining the initial as-etched pattern, it is necessary to keep θ between 33 ° and 16 °, while in order to suppress the generation of the facets acting as carrier leakage paths on the corner, θ must be kept between 53 ° and 29 °. Consequently, it was made clear that it is possible to grow GaAs and AlGaAs layers by MBE on the (001) triangle without modifying the initial as-etched pattern in the narrow θ range of 33 ° to 29 ° only. Figure 7 shows a top view of a 3.6 μm thick Si-doped GaAs layer grown under this θ condition. No appreciable modification to the as-etched pattern can be seen even for such thick layer growth. This result practically limits the choice of the sidewall orientation to (113)A ($\theta=30$ °). It is interesting to note that the growth, characterization, and device application of GaAs and AlGaAs layers and GaAs/AlGaAs quantum wells on the (113)A surface have recently attracted increasing attention for amphoteric Si doping and singular electronic properties [63-72]. It should be noted from Figure 3 that the interface of the layers grown on the (111)A substrate plane and sidewalls is flat and perpendicular to the substrate plane, that is, $[\bar{1}\bar{1}2]$A-oriented, irrespective of the

existence of the (114)A facet. This favorably contributes to the simplification of the structure of lateral (111)A - (113)A junctions. Moreover, as shown in Figure 4(f), the layer on the (113)A sidewall has an excellent surface morphology. Supported by these features specific to the growth on (111)A patterned substarates, an excellent current blocking effect was confirmed for Si-doped GaAs layers grown on the triangles with equivalent (113)A sidewalls [49-51], and excellent tunneling and light emitting characteristics of the lateral p-type (111)A - n-type (113)A subband junctions have been demonstrated [58].

2. (110) triangle

Figure 8 shows ($\bar{1}10$) cross-sectional views of the as-etched profiles of the (110)-related sidewalls with various values of θ. Figure 9 shows ($\bar{1}10$) cross-sectional views of the corresponding grown layers. Generation of extra facets on the sidewalls is described as follows:

(a) For $\theta \geqq 71°$, an extra ($11\bar{1}$)B facet with $\theta_f = 71°$ was generated.

(b)-(h) For $71° > \theta \geqq 30°$, the ($11\bar{1}$)B facet disappeared and, instead, an extra (110) facet with $\theta_f = 35°$ and an extra (113)A facet adjacent to the (110) facet appeared. The (110) facet continued to be present over a wide θ range, and hence, an important element to be controlled. The (110) facet developed more towards the sidewall as θ approached 35°, θ_f for this facet, like the (114)A facet on the (001) triangle. For $\theta = 37°$, (g), the whole sidewall was covered by the (110) facet. In contrast to the (114)A facet, the (110) facet was still present on the lower part of the sidewall for $\theta < 35°$, as shown in (h). The (113)A facet vanished once the (110) facet moved to the lower part of the sidewall.

(i)-(j) For $30° > \theta \geqq 16°$, the (110) facet finally disappeared and no extra facets were generated, leading to a flat and uniform sidewall that maintained the initial as-etched profile.

(k) For $\theta < 16°$, steps with $\theta_f = 16°$ appeared near the sidewall - substrate plane boundary.

Figures 10 shows bird's eye views of the growth behavior of the ($11\bar{1}$)B facet with respect to θ. The ($11\bar{1}$)B facet was not completely flat but exhibited mosaic

patterns. This may be attributed to the present growth conditions optimized for the (111)A surface (high temperature and high As_4 pressure), which did not match the optimum growth conditions for the $(\bar{1}\bar{1}\bar{1})$B surface (high temperature and low As_4 pressure) [23, 24, 26-31]. The supply of excess Ga atoms from the adjacent (111)A substrate plane, which will be discussed in a subsequent paper, designated as Paper III, however, reduced the effective V/III flux ratio and favorably contributed to the $(11\bar{1})$B facet growth. Note that only a 6 ° decrease in θ caused a qualitative change in the facet generation, as shown in (b).

Figures 11 shows bird's eye views of the growth behavior of the (110) facet with respect to θ. The surface of the (110) facet was relatively flat for for $\theta \geqq 49$ ° ((a) and (b)), whereas it tended to show the characteristic features reported in the literature [32-34, 37] as the (110) facet developed towards the sidewall with decreasing θ below 49 ° ((c)-(e)). After the (110) facet completely vanished for $\theta < 30$ °, the layers on the sidewall showed a smooth surface like that on the (113)A sidewall ((661)A, for example, shown in (f)). One interesting phenomenon is the formation of giant steps on the sidewalls with θ around θ_f of the (110) facet, of the same type as has been reported on misoriented planar (110) substrates in [73-75]. Figures 12(a) and (b) show the magnified (110) cross-sectional images corresponding to Figures 11(c) and (e), respectively. For $\theta = 40$ °, which corresponds to the (110) surface misoriented by 5 ° towards the $[11\bar{1}]$B direction, we observe giant steps with about 1.3 μm-wide terraces running in the $[\bar{1}10]$ direction below the (110) facet (Figure 11(c)) and the corresponding Al composition variation (seen as a lateral gradation in the AlGaAs layers in (a)). For $\theta = 32$ °, which corresponds to the (110) surface misoriented by 3 ° towards the [111]A direction, we observe giant steps with about 2.6 μm-wide terraces running in the $[\bar{1}10]$ direction above the (110) facet (Figure 11(e)) and the corresponding Al composition variation ((b)) as well. In contrast, such giant steps were not formed on the (001)-related sidewalls with θ around θ_f of the (114)A facet, as confirmed for $\theta = 41$ ° and 36 °, which respectively correspond to the (114)A surfaces misoriented by 9 ° (Figure 4(d) and Figure 12(c)) and 3 ° (Figure 4(e) and

Figure 12(d)) towards the [001] direction. This result may reflect the difference in the way Ga adatoms are incorporated between the (110) and (114)A planes, as is clearly evidenced by the large growth rate difference between them in Paper III.

Figure 13 shows top views of the as-etched profiles of the corners of the (110) triangles with various values of θ. These profiles cannot be distinguished from those for the (001) triangles shown in Figure 5. Figure 14 shows top views of the corners of the (110) triangles after growth. Although an incomplete facet-like structure was observed on the corner for $55° \geqq \theta > 39°$ ((e)-(f)), no definite extra facets developed on the corners of the (110) triangles, in distinct contrast to the (001) triangles discussed above.

Table 1 summarizes the facet generation behavior for the (110) triangle. In order to obtain flat and uniform layers that maintain the initial as-etched pattern, it is necessary to keep θ between 30° and 16°. The (661)A sidewall with $\theta = 28°$ is a good choice for that purpose. It should be noted from Figure 9 that the interface of the layers grown on the (111)A substrate plane and sidewall becomes flat and vertical to the substrate plane, that is, $[\bar{1}\bar{1}2]$A-oriented, after disappearance of the (110) facet for $\theta < 35°$. This favorably contributes to the simplification of the structure of lateral (111)A - (661)A junctions. This is similar to the situation with the (001) triangle. No current blocking effects, however, were confirmed for Si-doped GaAs layers grown on the (110) triangles with equivalent (661)A sidewalls [51] since Si-doped GaAs layers on the (NNM)A sidewalls show p-type conduction as well as those on the (111)A substrate plane, as was discussed in the previous section.

3. (201) triangle

Figure 15 shows $(\bar{1}10)$ cross-sectional views of the as-etched profiles of the (201)-related sidewalls with various values of θ. The $HF+H_2O_2+H_2O$ mixtures used produced an inverted mesa together with the normal sidewall for large θ. Since the (201) triangle does not intersect the $(\bar{1}10)$ cleavage plane at right angles as shown in Figure 1, the actual value of θ was evaluated from the experimentally observed apparent value, θ', on the SEM photographs using the

equation $\theta = \tan^{-1}(\tan\theta'/\cos 30°)$. Figure 16 shows $(\bar{1}10)$ cross-sectional views of the corresponding grown layers. Generation of extra facets on the sidewalls is described as follows:

(a)-(b) For θ around 70° with the inverted mesas, extra $(\bar{1}01)$ and (159) facets with $\theta_f = 90°$ and 34° were generated. It is an interesting phenomenon that the (159) facet generated at the initial stage of growth disappeared as the growth proceeded for the deeper inverted mesa shown in (a). This phenomenon was not observed either for the shallower inverted mesa shown in (b) or for the normal mesas shown below. This will be discussed later.

(c)-(e) For $72° \geqq \theta > 55°$, the $(\bar{1}01)$ facet disappeared and an extra $(\bar{2}38)$ facet with $\theta_f = 56°$ appeared. The (159) facet continued to be present.

(f)-(h) For $55° \geqq \theta \geqq 33°$, the $(\bar{2}38)$ facet disappeared and instead an extra $(\bar{1}25)$ facet with $\theta_f = 49°$ appeared. The (159) facet developed more towards the sidewall as θ became closer to 34°, θ_f for this facet, like the (114)A facet on the (001) triangle and the (110) facet on the (110) triangle. The $(\bar{1}25)$ facet was pushed down on the sidewall by the (159) facet development with decreasing θ. The (159) facet, which exists over a wide θ range, is thus an important element to be controlled. The generation of the $(\bar{1}25)$ facet is interesting in that the facet exists on the sidewalls with $\theta < \theta_f$ of the facet, like the (110) facet.

(i)-(j) For $33° > \theta > 17°$, the (159) and $(\bar{1}25)$ facets finally disappeared and no extra facets were generated, leading to a sidewall that maintained the initial as-etched profile, although its flatness and uniformity were inferior to those for the (001) and (110) triangles.

(k) For $\theta < 17°$, steps with $\theta_f = 17°$ appeared near the sidewall - substrate boundary. This is the same behavior as observed for the (001) and (110) triangles.

Figure 17 shows bird's eye views of the growth behavior of the $(\bar{1}01)$ facet with respect to θ. Since the $(\bar{1}01)$ facet did not appear on the sidewalls consisting only of normal mesas with similar θ values ((c) and Figure 16(c)), it is concluded that the $(\bar{1}01)$ facet generation depended on the presence of the inverted mesa. This

result and the behavior of the (159) facet mentioned above suggest that the Ga adatom migration is greatly influenced by the profile between the substrate plane and the sidewall.

Figure 18 shows bird's eye views of the growth behavior of the (159) facet with respect to θ. The characteristic surface morphology of the (159) facet is clearly observed and does not change with θ. The development of the (159) facet towards the sidewall with decreasing θ is also clearly observed. After the (159) facet has completely vanished for $\theta \leqq 32°$, the layer on the sidewall shows a relatively good surface morphology as exemplified by the (135) sidewall layer ((f)) although poorer than the (113)A and (661)A sidewall layers.

Figure 19 shows top views of the as-etched profiles of the corners of the (021) triangles with various values of θ. Again, these profiles cannot be distinguished from those for the (001) or (110) triangles shown in Figures 5 and 13. Figure 20 shows top views of the corners of the (021) triangles after growth. Generation of extra facets on the corners is described as follows:

(a) For θ around 70° with the deep inverted mesa, no definite extra facets were seen on the corner.

(b)-(e) For the shallow inverted mesa shown in (b) and for the normal sidewalls with $72° \geqq \theta \geqq 51°$ shown in (c)-(e), an extra (110) facet started to develop and increasingly grew towards the bottom of the corner with decreasing θ.

(f)-(i) Once θ decreased below 51°, however, the (110) facet decomposed into two parts which have orientations more associated with the two intersecting sidewalls. For $51° > \theta \geqq 26°$, No extra facets were generated on the corner and a definite intersection line existed there.

(j)-(l) Below $\theta = 26°$, the (NNM)A facets (N=2, 3, --; M≧N/2) appeared.

The (110) and (NNM)A facets described above were identified in the same way as those for the (001) triangle: The orientation of these facets were exactly the same as those on the (001) triangles. The angle projected on the $(\bar{1}10)$ plane, θ_c', of the intersection line to the (111)A substrate plane was evaluated from the experimentally determined value of θ using the simple relation $\theta_c' = \tan^{-1}$

($\tan\theta/\sqrt{3}$). The value of $\theta_c'=35°$ corresponding to θ_f of the (110) facet corresponds to $\theta=51°$. This calculation coincides well with the experimental result that the facet appearing on the corner for $\theta\geqq51°$ disappeared for $\theta<51°$ and confirms that the facet in question is really (110)-oriented. The value of $\theta=26°$, corresponding to the existence boundary of the (NNM)A facets gives the value of $\theta_c=16°$. This value corresponds to θ_f of the (221)A plane. The (NNM)A facets shown in Figures 20(j), (k), (l) correspond to (774)A, (885)A, and (443)A, respectively. These results are similar to those obtained for the (001) triangles.

Table 1 summarizes the facet generation behavior for the (201) triangle. In order to obtain flat and uniform layers on the sidewall that maintain the initial as-etched pattern, it is necessary to keep θ between 33° and 17°, while in order to suppress the generation of the facets acting as carrier leakage paths on the corner, θ must be kept between 51° and 26°. Consequently, it was made clear that it is possible to grow GaAs and AlGaAs layers by MBE on (201) triangles without modifying the initial as-etched patterns in the narrow θ range of 33° to 26° only. This situation is similar to that for the (001) triangle. The (135) sidewall with $\theta=29°$ is the candidate most suitable for that purpose.

It should be noted that the interface of the layers grown on the (111)A substrate plane and sidewalls is flat and perpendicular to the substrate plane, that is, [$\bar{1}$01]-oriented, irrespective of the existence of the extra facets shown above. This, again, favorably contributes to the simplification of the structure of, for example, lateral (111)A - (135) junctions. An excellent current blocking effect comparable to the (001) triangles with equivalent (113)A sidewalls has been confirmed for Si-doped GaAs layers grown on the (201) triangles with equivalent (135) sidewalls [76]. Si-doped GaAs layers grown on (012) substrates by MBE have been reported to show n-type conduction comparable to those simultaneously grown on (001) substrates [31]. Since the (135) plane is oriented by 11° more towards the [111]A direction than the (012) plane and the (111)A surface shows p-type conduction by Si-doping, it is expected to be more difficult to obtain n-type conduction on the (135) plane by Si-doping. The present result has revealed that

the (135) layer actually shows n-type conduction by Si-doping as well as the (113)A layer, at least under the present growth conditions.

4. Phenomena common to three triangle patterns

Although the three triangles showed their respective facet generation behaviors as discussed above, the following points are worth mentioning as common to the three triangles.

(1) The persistent extra facets generating on the three triangles, that is, the (114)A facet on the (001) triangle, the (110) facet on the (110) triangle, and the (159) facet on the (201) triangle, have θ_f in the narrow range of 33 ° to 35 °.

(2) The steps with θ_f=16 °-17 ° appear near the sidewall - substrate plane boundary. They correspond to the (447)A surface for the (001) triangle, the (221)A surface for the (110) triangle, and the (5 8 11) surface for the (201) triangle.

These points seem to be related to the crystal structure of GaAs composed of tetrahedral Ga-As bonding and are under study.

5. (110)-related facet generation and (111)A surface morphologies

Figure 21 shows pyramidal microstructures with (110)-related facets frequently observed on GaAs and AlGaAs layers grown on exact (111)A substrates [53, 56]. Figure 22 shows step structures consisting of the equivalent (011)-related and (101)-related facets (not the (001) facet !) on GaAs and AlGaAs layers on (111)A substrates misoriented towards the [001] direction and those consisting of the (110)-related facets on GaAs and AlGaAs layers on (111)A substrates misoriented toward the [110] direction. The preferential generation of the (110) and (NNM)A facets on the corners of the (001) and (201) triangles elucidated in the present paper is closely related to the development of these (110)-related structures and strongly suggests the special importance of these planes as fundamental growth elements in the MBE growth of GaAs and AlGaAs on (111)A substrates.

6. Misorientation effects

Finally, we would like to discuss the effects of the usage of substrates misoriented from the (111)A direction on the growth behavior on the triangle

patterns. Figure 23 shows 1μm thick Si-doped GaAs layers grown on (a) a (110) triangle with equivalent (661)A side walls and (b) a (001) triangle with equivalent (113)A side walls formed on a (111)A substrate misoriented by 3 ° towards the [001] direction. The following points can be noted:

(1) The (110) triangle

Step structures consisting of the equivalent (011)-related and (101)-related facets appeared at the substrate - (661)A sidewall boundary (①) and faded towards the $[\bar{1}\bar{1}2]$A direction with a background morphology characteristic of 3 ° misorientation towards the [001] direction shown in Figure 22.

(2) The (001) triangle

Step structures consisting of the (011)-related facets appeared at the substrate - (311)A sidewall boundary (②) and those consisting of the (101)-related facets appeared at the substrate - (131)A sidewall boundary (③). They faded towards the $[2\bar{1}\bar{1}]$A and $[\bar{1}2\bar{1}]$A directions, respectively, with a background morphology characteristic of 3 ° misorientation towards the [001] direction shown in Figure 22. A (110)-related facet developed on the corner pointing in the $[11\bar{2}]$B direction (④) and no such facets developed on the other two corners.

Similar phenomena were observed for a (111)A substrate misoriented by 1 ° towards the [001] direction. The directional generation of the step structures clearly reflects the nonequivalent sidewalls and the directional migration of adatoms between the substrate plane and sidewalls caused by the misorientation. Consequently, mirror-like surfaces without steps can be obtained on the substrate plane only for exact (111)A substrates (within ± 0.1 °) in the growth on ridge-type triangles.

4. Summary and Conclusion

Extra facet generation during MBE growth of GaAs/AlGaAs multilayers on exact (111)A GaAs substrates patterned with ridge-type triangles with (001)-related, (110)-related, and (201)-related sidewalls, designated as "(001) triangle", "(110) triangle", and "(201) triangle", respectively, has been investigated for the

first time. Generation of extra $(\bar{1}\bar{1}3)$A, (001), and (114)A facets has been confirmed on the (001)-related sidewalls, extra $(11\bar{1})$B, (110), and (113)A facets on the (110)-related sidewalls, and extra $(\bar{1}01)$, $(\bar{2}38)$, $(\bar{1}25)$, and (159) facets on the (201)-related sidewalls, depending on the intersection angle θ of the sidewall and the substrate plane. Of these, the (114)A, (110), and (159) facets are impotant because they persist over a wide range of θ and, therefore, play a detrimental role in forming flat and uniform sidewall layers on the (111)A patterned substrates. The (110) and (NNM)A (N=2, 3, --; M≧N/2) have developed on the corners of the (001) and (201) triangles, while no extra facets have developed on the corners of the (110) triangles. It has been made clear that no extra facets are generated on the sidewalls or corners and flat and uniform layers maintaining the initial as-etched triangle patterns can be grown for the (001) triangles with $33\,^{\circ} \geqq \theta \geqq 29\,^{\circ}$, the (110) triangles with $30\,^{\circ} \geqq \theta \geqq 16\,^{\circ}$, and the (201) triangles with $33\,^{\circ} \geqq \theta \geqq 26\,^{\circ}$. Pyramidal microstructures with equivalent (110)-related facets on GaAs and AlGaAs layers grown on planar exact (111)A substrates and step structures composed of equivalent (110)-related facets on GaAs and AlGaAs layers grown on misoriented (111)A substrates has been suggested to be closely related to the preferential generation of the (110) and (NNM)A facets found in the present study. Formation of giant steps on the (110)-related side walls adjacent to the (110) facet when θ is close to the facet angle of the (110) facet has been reported. Nonuniform growth on the triangular (111)A substrate plane and asymmetric generation of the $(11\bar{0})$-related facets on the corners when misoriented (111)A substrates were used, have been presented.

-ACKNOWLEDGMENTS-

The authors would like to thank Dr. Y. Furuhama for his encouragement throughout this work.

-REFERENCES-

[1] W. T. Tsang and A. Y. Cho, Appl. Phys. Lett. **30**, 293 (1977).

[2] J. S. Smith, P. L. Derry, S. Margalit, and A. Yariv, Appl. Phys. Lett. **47**, 712 (1985).

[3] D. L. Miller, Appl. Phys. Lett. **47**, 1309 (1985).

[4] T. Yuasa, M. Manno, T. Yamada, S. Narituka, K. Shinozaki, and M. Ishii, J. Appl. Phys. **62**, 764 (1987).

[5] E. Kapon, M. C. Tamargo, and D. M. Hwang, Appl. Phys. Lett. **50**, 347 (1987).

[6] H. P. Meier, R. F. Broom, P. W. Epperlein, E. van Gieson, Ch. Harder, H. Jäckel, W. Walter, and D. J. Webb, J. Vac. Sci. Technol. B **6**, 692 (1987).

[7] H. P. Meier, E. van Gieson, R. F. Broom, W. Walter, D. J. Webb, C. Harder, and H. Jäckel, Inst. Phys. Conf. Ser. No.**91**, 609 (1988).

[8] S. Nilsson, E. van Gieson, D. J. Arent, H. P. Meier, W. Walter, and T. Forster, Appl. Phys. Lett. **55**, 972 (1989).

[9] D. J. Arent, S. Nilsson, Y. D. Galeuchet, H. P. Meier, and W. Walter, Appl. Phys. Lett. **55**, 2611 (1989).

[10] M. Hata, T. Isu. A. Watanabe, and Y. Katayama, Appl. Phys. Lett. **56**, 2542 (1990).

[11] M. Hata, T. Isu. A. Watanabe, and Y. Katayama, J. Vac. Sci. Technol. B **8**, 692 (1990).

[12] Y. Nakamura, S. Koshiba, M. Tsuchiya, H. Kano, and H. Sakaki, Appl. Phys. Lett. **59**, 700 (1991).

[13] X. Q. Shen, M. Tanaka, and T. Nishinaga, 10th Symp. Rec. Alloy Semicond. Phys. Electron. 65 (1991).

[14] S. Shimomura, S. Ohkubo, Y. Yuba, S. Namba, S. Hiyamizu, M. Shigeta, T. Yamamoto, and K. Kobayashi, Surf. Sci. **267**, 13 (1992).

[15] Y. Morishita, Y. Momura, S. Goto, Y. Katayama, and T. Isu, Inst. Phys. Conf. Ser. No.**120**, 19 (1992).

[16] X. Q. Shen, M. Tanaka, and T. Nishinaga, 11th Symp. Rec. Alloy Semicond. Phys. Electron. 333 (1992).

[17] X. Q. Shen and T. Nishinaga, 12th Symp. Rec. Alloy Semicond. Phys. Electron. 367 (1993).

[18] M. Walther, T. Röhr, G. Böhm, G. Tränkle, and G. Weimann, J. Crystal Growth **127**, 1045 (1993).

[19] H. Saito, M. Sugimoto, M. Anan, Y. Ochiai, Jpn. J. Appl. Phys. **32**, L1034 (1993).

[20] X. Q. Shen and T. Nishinaga, Jpn. J. Appl. Phys. **32**, L1117 (1993).

[21] T. Hayakawa, M. Kondo, T. Suyama, K. Takahashi, S. Yamamoto, and T. Hijikata, Jpn. J. Appl. Phys. **26**, L302 (1987).

[22] H. Imamoto, F. Sato, K. Imanaka, and M. Shimura, Appl. Phys. Lett. **55**, 115 (1989).

[23] K. Tsutsui, H. Mizukami, O. Ishiyama, S. Nakamura, and S. Furukawa, Jpn. J. Appl. Phys. **29**, 468 (1990).

[24] P. Chen, K. C. Rajkumar, and A. Madhukar, Appl. Phys. Lett. **58**, 1771 (1991).

[25] A. Chin, P. Martin, P. Ho, J. Ballingall, T. -H. Yu, and J. Mazurowski, Appl. Phys. Lett. **59**, 1899 (1991).

[26] T. Hayakawa, M. Nagai, M. Morishima, H. Horie, and K. Matsumoto, Appl. Phys. Lett. **59**, 2287 (1991).

[27] T. Hayakawa, M. Morishima, and S. Chen, Appl. Phys. Lett. **59**, 3321 (1991).

[28] T. Hayakawa, M. Morishima, M. Nagai, H. Horie, and K. Matsumoto, Surf. Sci. **267**, 8 (1992).

[29] J. Fu, K. Zhang, and D. L. Miller, J. Vac. Sci. Technol. B **10**, 779 (1992).

[30] D. A. Woolf, Z. Sobiesierski, D. I. Westwood, and R. H. Williams, J. Appl. Phys. **71**, 4908 (1992).

[31] D. A. Woolf, J. P. Williams, D. I. Westwood, Z. Sobiesierski, J. E. Aubrey, and R. H. Williams, J. Crystal Growth **127**, 913 (1993).

[32] J. M. Ballingall and C. E. C. Wood, Appl. Phys. Lett. **41**, 947 (1982).

[33] W. I. Wang, J. Vac. Sci. Technol. B 1, 630 (1983).

[34] L. T. Parechanian, E. R. Weber, T. L. Hierl, Mat. Res. Soc. Symp. Proc. **46**, 391 (1985).

[35] Z. Junming, H. Yi, L. Yongkang, and J. W. Yi, J. Crystal Growth **81**, 221 (1987).

[36] L. T. P. Allen, E. R. Weber, J. Washburn, and Y. C. Pao, Appl. Phys. Lett. **51**, 670 (1987).

[37] L. T. P. Allen, E. R. Weber, J. Washburn, Y. C. Pao, and A. G. Elliot, J. Crystal Growth **87**, 193 (1988).

[38] L. Pfeiffer, K. W. West, H. L. Stromer, J. P. Eizenstein, K. W. Baldwin, D. Gershoni, and J. Spector, Appl. Phys. Lett. **56**, 1697 (1990).

[39] M. López, Y. Takano, K. Pak, and H. Yonezu, Appl. Phys. Lett. **58**, 580 (1991).

[40] G. Tanaka, K. Hirakawa, H. Ichinose, and T. Ikoma, Inst. Phys. Conf. Ser. No.**120**, 25 (1992).

[41] S. Fuke, M. Umemura, N. Yamada, K. Kuwahara, and T. Imai, J. Appl. Phys. **68**, 97 (1990).

[42] Y. Kadoya, A. Sato, H. Kano, and H. Sakaki, J. Crystal Growth **111**, 280 (1991).

[43] M. Umemura, K. Kuwahara, S. Fuke, M. Sato, and T. Imai, J. Appl. Phys. **72**, 313 (1992).

[44] M. R. Fahy, J. H. Neave, M. J. Ashwin, R. Murray, R. C. Newman, B. A. Joyce, Y. Kadoya, and H. Sakaki, J. Crystal Growth **127**, 871 (1993).

[45] Y. Okano, H. Seto, H. Katahama, S. Nishine, I. Fujimoto, and T. Suzuki, Jpn. J. Appl. Phys. **28**, L151 (1989).

[46] Y. Okano, M. Shigeta, H. Seto, H. Katahama, S. Nishine, and I. Fujimoto, Jpn. J. Appl. Phys. **29**, L1357 (1990).

[47] M. Shigeta, Y. Okano, H. Seto, H. Katahama, S. Nishine, K. Kobayashi, and I. Fujimoto, J. Crystal Growth **111**, 284 (1991).

[48] T. Yamamoto, M. Fujii, T. Takebe, D. Lovell, and K. Kobayashi, Inst. Phys. Conf. Ser. No.120, 31 (1992).

[49] M. Fujii, T. Yamamoto, M. Shigeta, T. Takebe, K. Kobayashi, S. Hiyamizu, and I. Fujimoto, Surf. Sci. **267**, 26 (1992).

[50] M. Fujii, T. Takebe, T. Yamamoto, M. Inai, and K. Kobayashi, Superlattices and Microstructures 12, 167 (1992).

[51] K. Kobayashi, T. Takebe, T. Yamamoto, M. Fujii, M. Inai, and D. Lovell, J. Electron. Mat. **22**, 161 (1993).

[52] K. Fujita, A. Shinoda, M. Inai, T. Yamamoto, M. Fujii, D. Lovell, T. Takebe, and K. Kobayashi, J. Crystal Growth **127**, 50 (1993).

[53] T. Yamamoto, M. Inai, T. Takebe, M. Fujii, and K. Kobayashi, J. Crystal Growth **127**, 865 (1993).

[54] T. Takebe, M. Fujii, T. Yamamoto, K. Fujita, and K. Kobayashi, J. Crystal Growth **127**, 937 (1993).

[55] A. Shinoda, T. Yamamoto, M. Inai, T. Takebe, M. Fujii, and K. Kobayashi, Inst. Phys. Conf. Ser. **129**, 495 (1993).

[56] T. Yamamoto, M. Inai, T. Takebe, and T. Watanabe, J. Vac. Sci. Technol. A 11, 631 (1993).

[57] M. Inai, T. Yamamoto, M. Fujii, T. Takebe, and K. Kobayashi, Jpn. J. Appl. Phys. **32**, 523 (1993).

[58] T. Yamamoto, M. Inai, T. Takebe, and T. Watanabe, Jpn. J. Appl. Phys. **32**, L28 (1993).

[59] K. Fujita, T. Yamamoto, T. Takebe, and T. Watanabe, Jpn. J. Appl. Phys. **32**, L978 (1993).

[60] T. Takebe, T. Yamamoto, M. Fujii, and K. Kobayashi, J. Electrochem. Soc. 140, 1169 (1993).

[61] T. Yamamoto, M. Inai, A. Shinoda, T. Takebe, and T. Watanabe, Jpn. J. Appl. Phys. **32**, 3346 (1993).

[62] P. N. Uppal, J. S. Ahearn, and D. P. Musser, J. Appl. Phys. **62**, 3766 (1987).

[63] W. I. Wang, E. E. Mendez, T. S. Kuan, and L. Esaki, Appl. Phys. Lett. **47**, 826 (1985).

[64] W. I. Wang, E. E. Mendez, Y. Iye, B. Lee, M. H. Kim, and G. E. Stillman, J. Appl. Phys. **60**, 1834 (1986).

[65] T. Takamori, T. Fukunaga, J. Kobayashi, K. Ishida, and H. Nakashima, Jpn. J. Appl. Phys. **26**, 1097 (1987).

[66] T. Fukunaga, T. Takamori, and H. Nakashima, J. Crystal. Growth **81**, 85 (1987).

[67] S. S. Bose, B. Lee, M. H. Kim, G. E. Stillman, and W. I. Wang, J. Appl. Phys. **63**, 743 (1988).

[68] T. Takamori, K. Watanabe, and T. Fukunaga, Electron. Lett. **27**, 729 (1991).

[69] W. Q. Li, P. K. Bhattacharya, S. H. Kwok, and R. Merlin, J. Appl. Phys. **72**, 3129 (1992).

[70] R. Nötzel and K. Ploog, J. Vac. Sci. Technol. A **10**, 617 (1992).

[71] E. C. Valadares, Phys. Rev. B **46**, 3935 (1992).

[72] R. K. Heyden, E. C. Valadares, M. Henini, L. Eaves, D. K. Maude, and J. C. Portal, Phys. Rev. B **46**, 15586 (1992).

[73] M. Sato, K. Maehashi, H. Asahi, S. Hasegawa, and H. Nakashima, Superlattices and Microstructures **7**, 279 (1990).

[74] S. Hasegawa, K. Kimura, M. Sato, K. Maehashi, and H. Nakashima, Surf. Sci. **267**, 5 (1992).

[75] K. Inoue, K. Kimura, K. Maehashi, S. Hasegawa, and H. Nakashima, J. Crystal Growth **127**, 1041 (1993).

[76] M. Inai, T. Yamamoto, M. Fujii, D. Lovell, T. Takebe, and K. Kobayashi, unpublished.

-FIGURE CAPTIONS-

Figure 1 Schematic presentation of ridge-type (001), (110), (201), and (021) triangles formed on the GaAs (111)A surface.

Figure 2 ($\bar{1}10$) cross-sectional views of the as-etched profiles of the (001)-related sidewalls with various slopes.

Figure 3 ($\bar{1}10$) cross-sectional views of the after-growth profiles of the (001)-related sidewalls corresponding to Figure 2.

Figure 4 Bird's eye views of the growth behavior of the (114)A facet (indicated by arrow) with respect to θ.

Figure 5 Top views of the as-etched profiles of the corners of the (001) triangles with various sidewall slopes.

Figure 6 Top views of the after-growth profiles of the corners of the (001) triangles corresponding to Figure 5.

Figure 7 Top view of a 3.6 μm thick Si-doped GaAs layer grown on the (001) triangle with equivalent (113)A sidewalls.

Figure 8 ($\bar{1}10$) cross-sectional views of the as-etched profiles of the (110)-related sidewalls with various slopes.

Figure 9 ($\bar{1}10$) cross-sectional views of the after-growth profiles of the (110)-related sidewalls corresponding to Figure 8.

Figures 10 Bird's eye views of the growth behavior of the ($11\bar{1}$)B facet (indicated by arrow) with respect to θ.

Figures 11 Bird's eye views of the growth behavior of the (110) facet (indicated by arrow) with respect to θ.

Figures 12 Magnified ($\bar{1}10$) cross-sectional views of (a) and (b) the (110)-related sidewalls with slopes around the facet angle of the (110) facet and (c) and (d) the (001)-related sidewalls with slopes around the facet angle of the (114)A facet.

Figure 13 Top views of the as-etched profiles of the corners of the (110) triangles with various sidewall slopes.

Figure 14 Top views of the after-growth profiles of the corners of the (110) triangles corresponding to Figure 13.

Figure 15 ($\bar{1}10$) cross-sectional views of the as-etched profiles of the (201)-related sidewalls with various slopes.

Figure 16 ($\bar{1}10$) cross-sectional views of the after-growth profiles of the (201)-related sidewalls corresponding to Figure 15.

Figure 17 Bird's eye views of the growth behavior of the ($\bar{1}01$) facet (indicated by arrow) with respect to θ.

Figure 18 Bird's eye views of the growth behavior of the (159) facet (indicated by arrow) with respect to θ.

Figure 19 Top views of the as-etched profiles of the corners of the (021) triangles with various sidewall slopes.

Figure 20 Top views of the after-growth profiles of the corners of the (021) triangles corresponding to Figure 19.

Figure 21 Pyramidal microstructures with (110)-related facets frequently observed on GaAs and AlGaAs layers grown on exact (111)A substrates.

Figure 22 (110)-related step structures on GaAs and AlGaAs layers grown on misoriented (111)A substrates.

Figure 23 1μm thick Si-doped GaAs layers grown on (a) a (110) triangle and (b) a (001) triangle on a (111)A substrate misoriented by 3 ° towards the [001] direction.

-TABLE HEADINGS-

Table 1 Summary of facet generation behavior during MBE on GaAs (111)A patterned substrates.

RIDGE-TYPE TRIANGLES ON GaAs (111)A SUBSTRATES

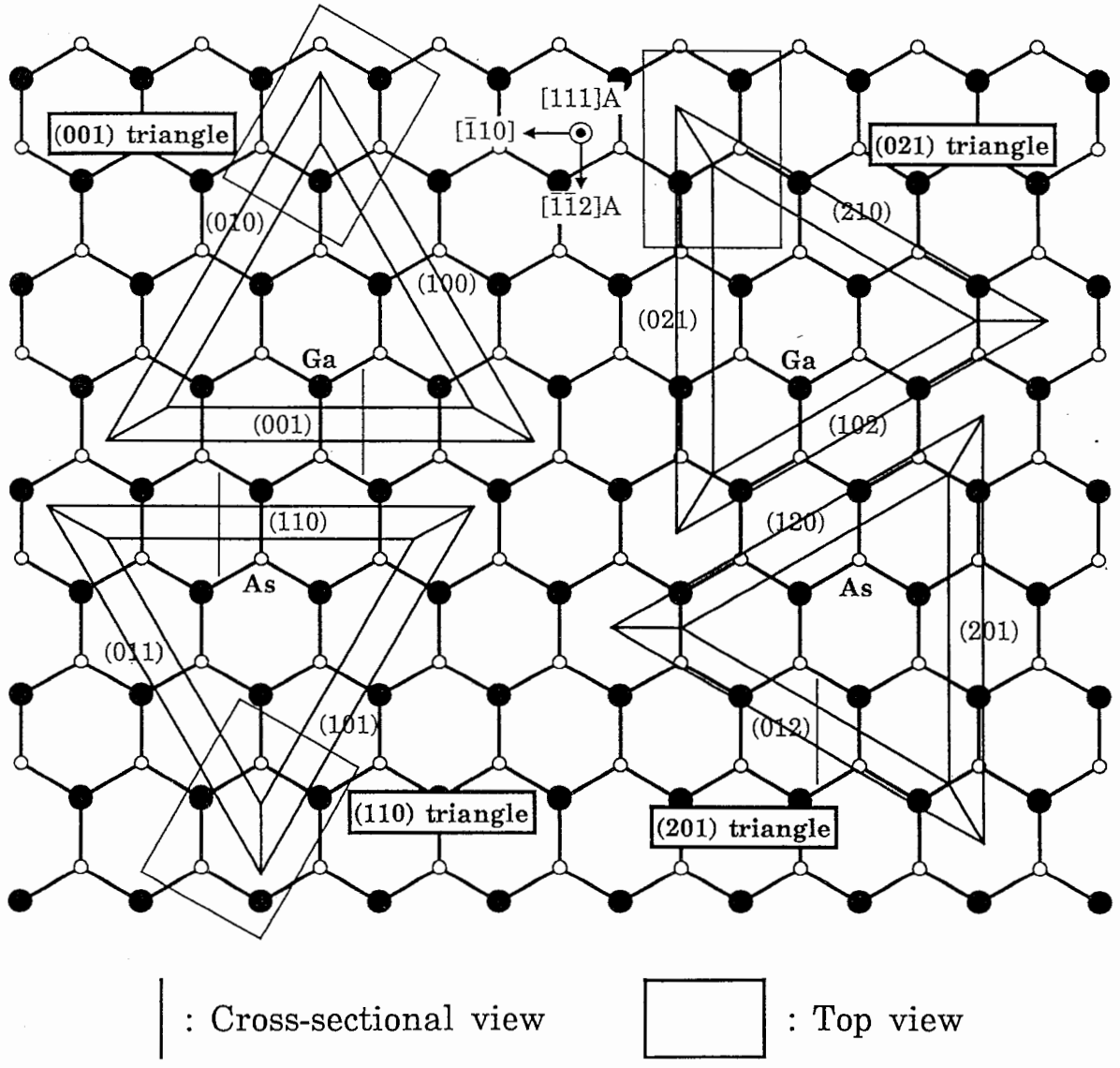

Figure 1 Schematic presentation of ridge-type (001), (110), (201), and (021) triangles formed on the GaAs (111)A surface.

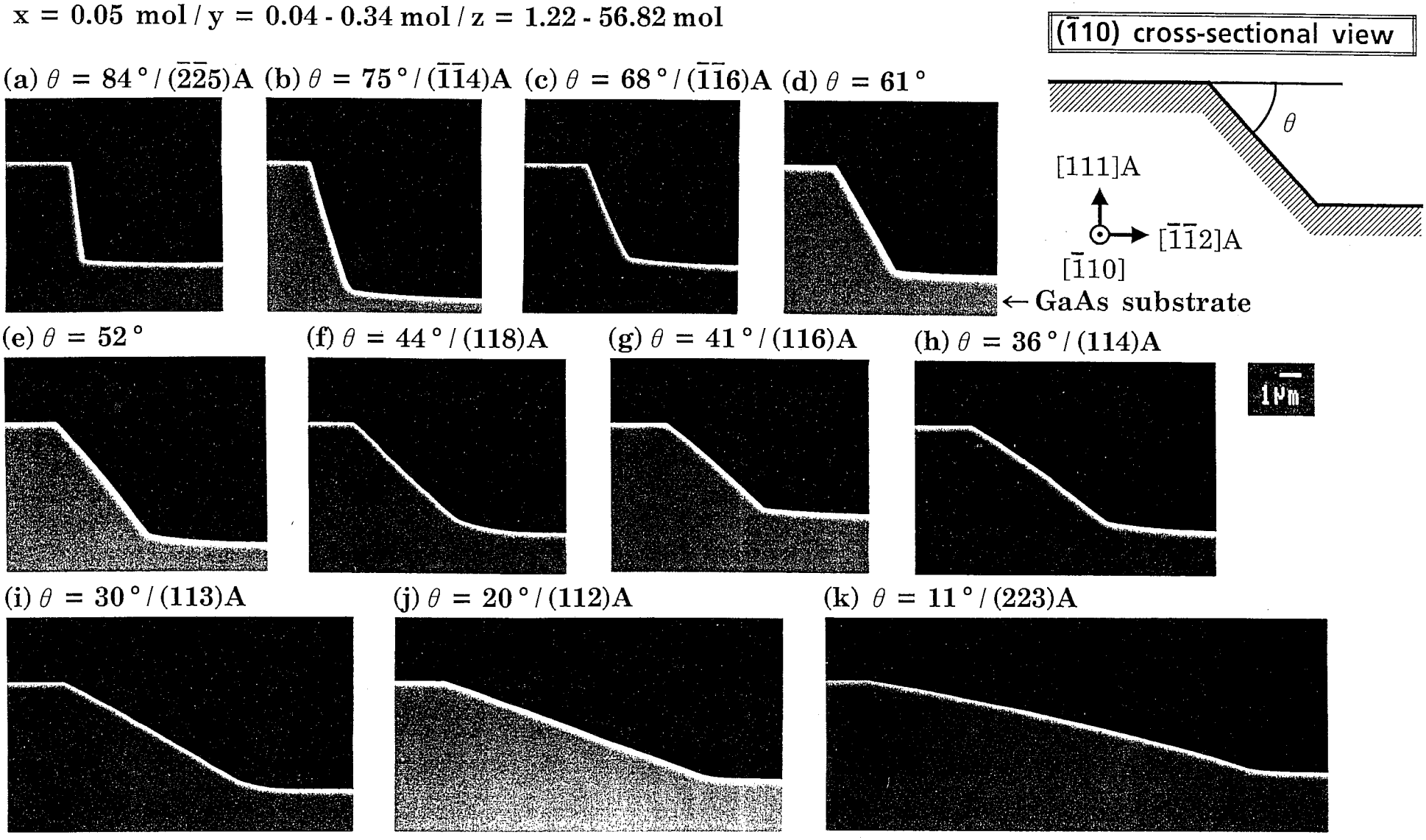

Figure 2 (1̄10) cross-sectional views of the as-etched profiles of the (001)-related sidewalls with various slopes.

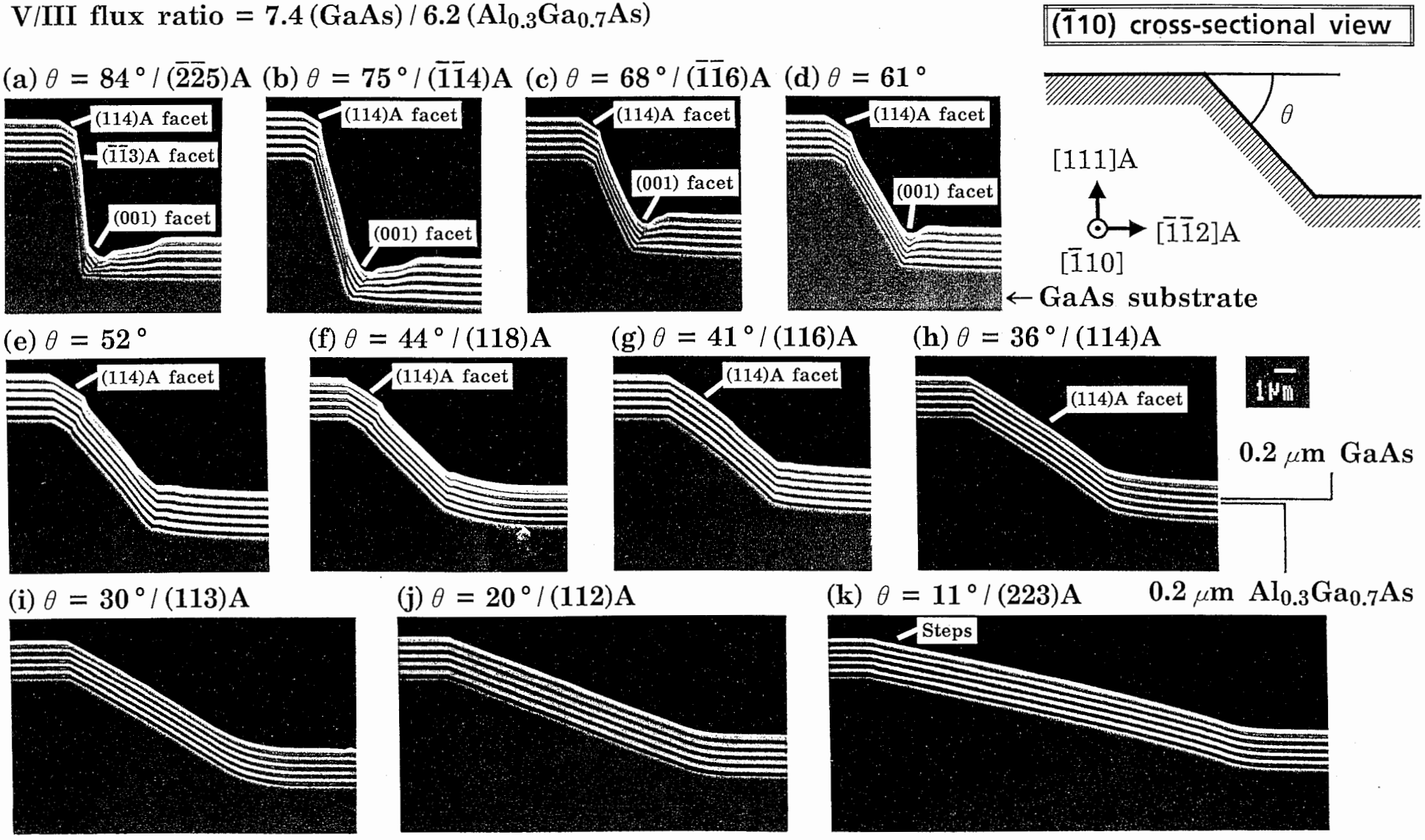

Figure 3 ($\bar{1}$10) cross-sectional views of the after-growth profiles of the (001)-related sidewalls corresponding to Figure 2.

(114)A / θ_f = 33 °

(a) θ = 84 ° / ($\bar{2}\bar{2}5$)A

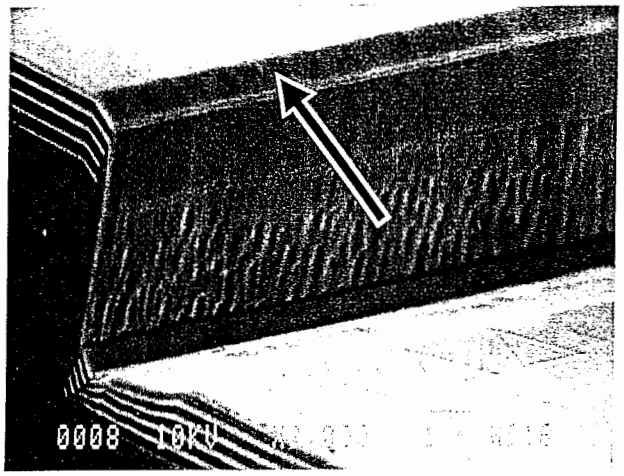

(b) θ = 68 ° / ($\bar{1}\bar{1}6$)A

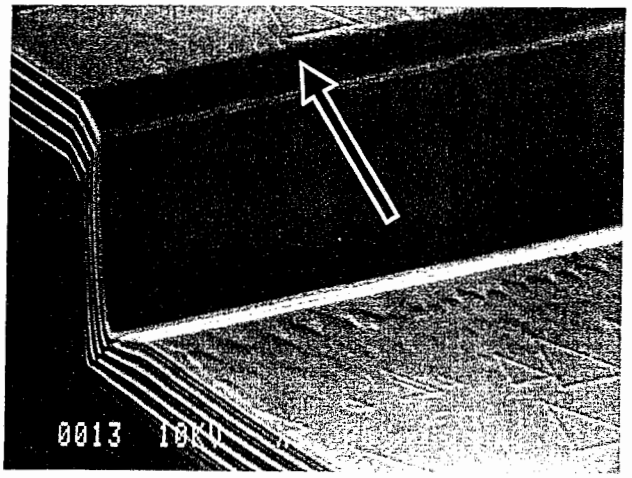

(c) θ = 52 °

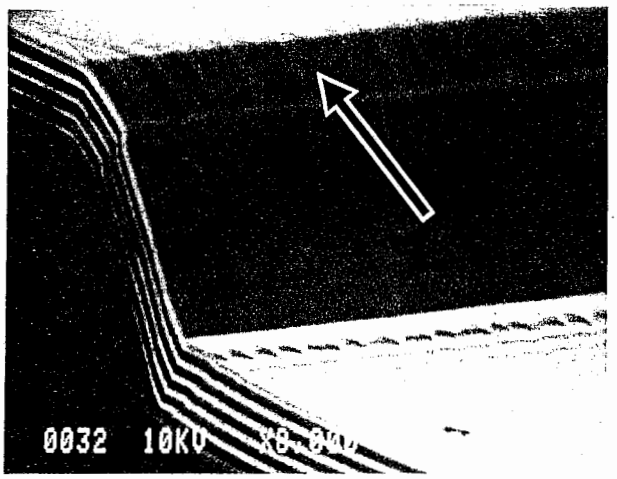

(d) θ = 41 ° / (116)A

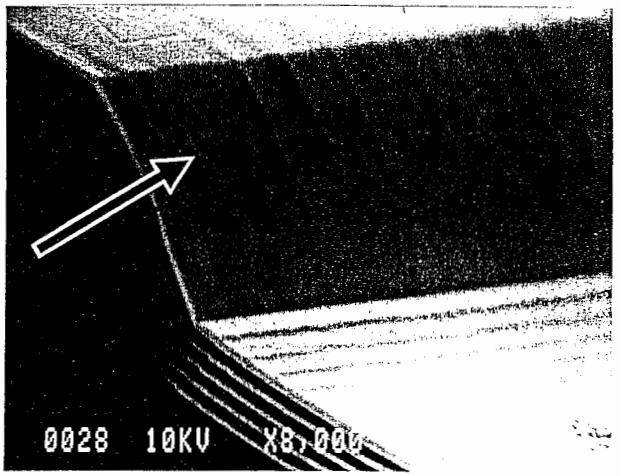

(e) θ = 36 ° / (114)A

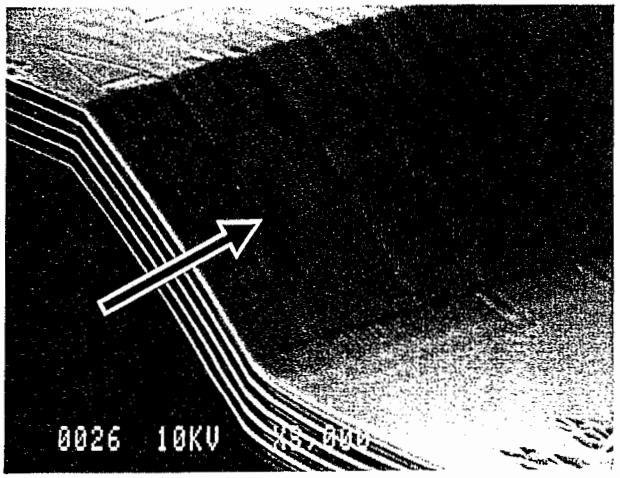

(f) θ = 30 ° / (113)A

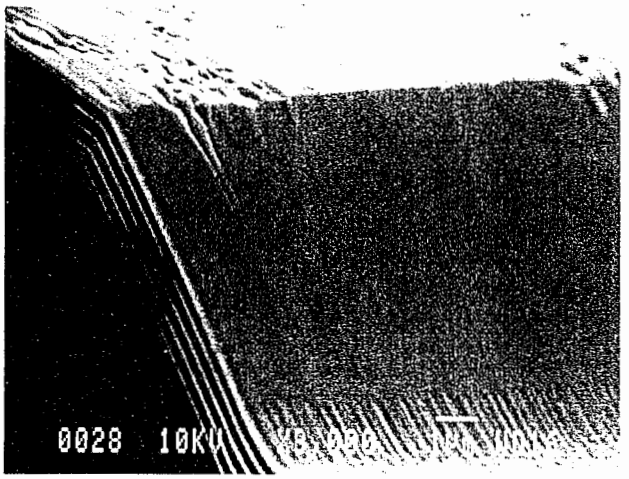

Figure 4 Bird's eye views of the growth behavior of the (114)A facet (indicated by arrow) with respect to θ.

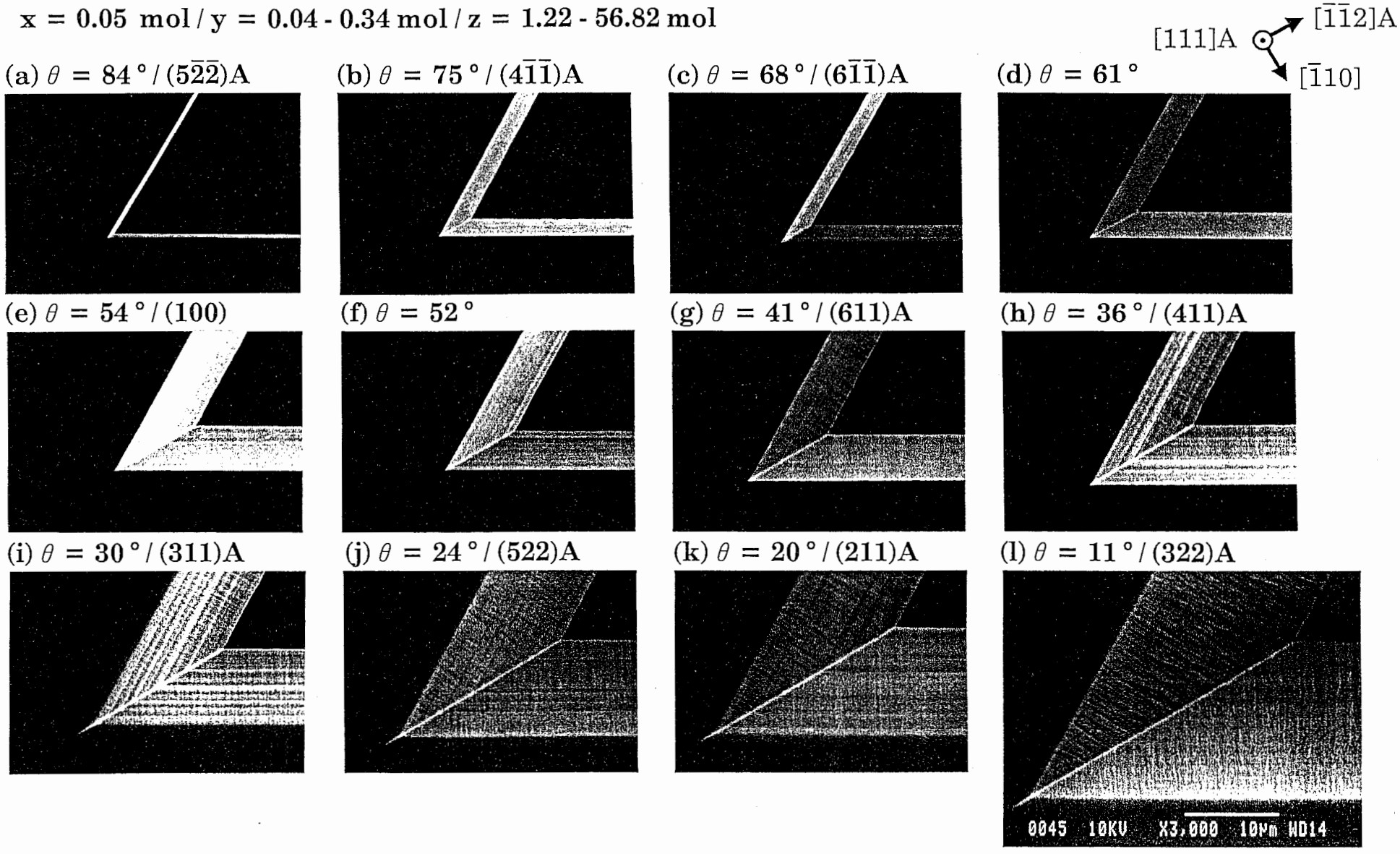

Figure 5 Top views of the as-etched profiles of the corners of the (001) triangles with various sidewall slopes.

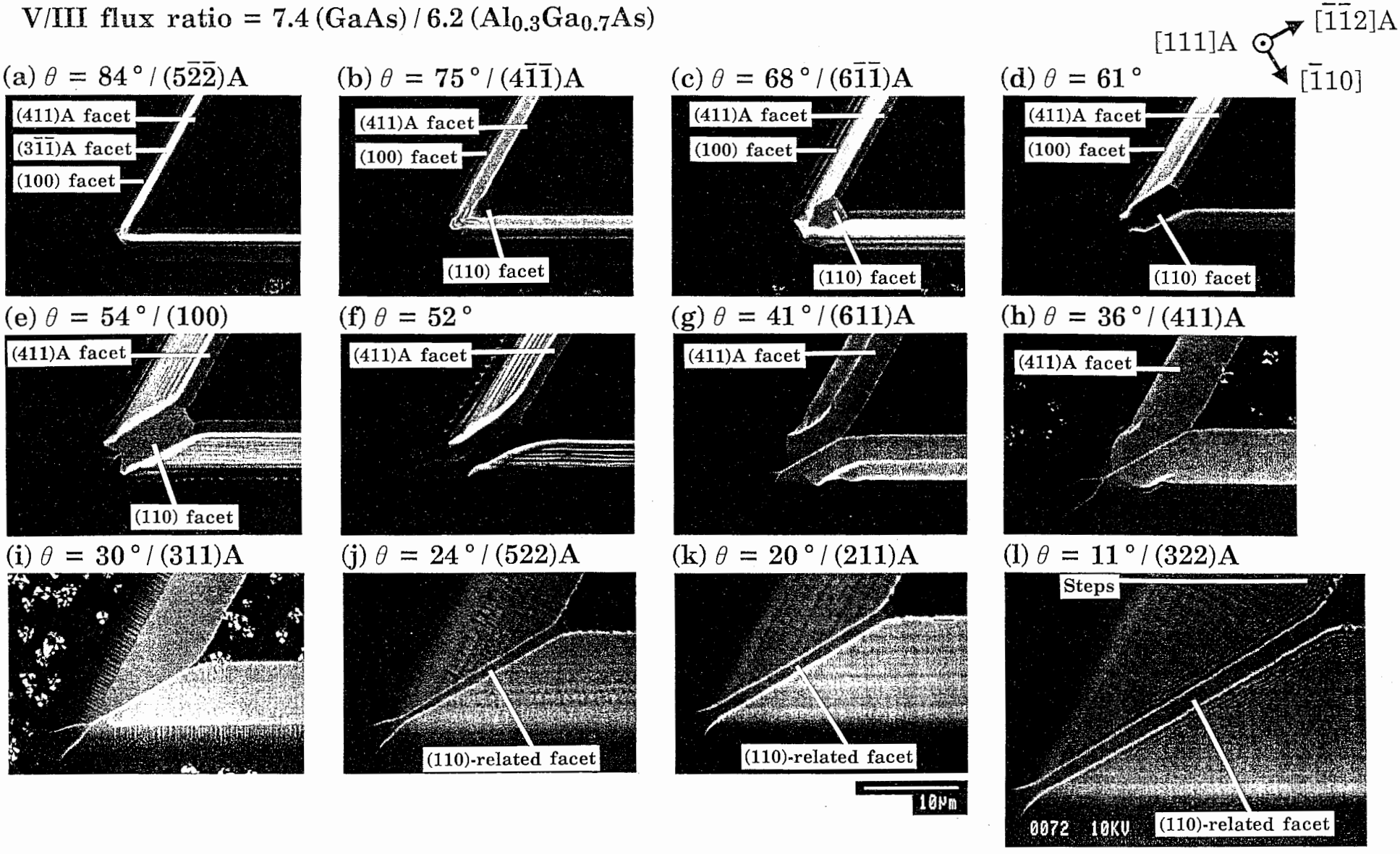

Figure 6 Top views of the after-growth profiles of the corners of the (001) triangles corresponding to Figure 5.

Thickness = 3.6 μm

"(001) triangle" : θ = 30 ° / (113)A

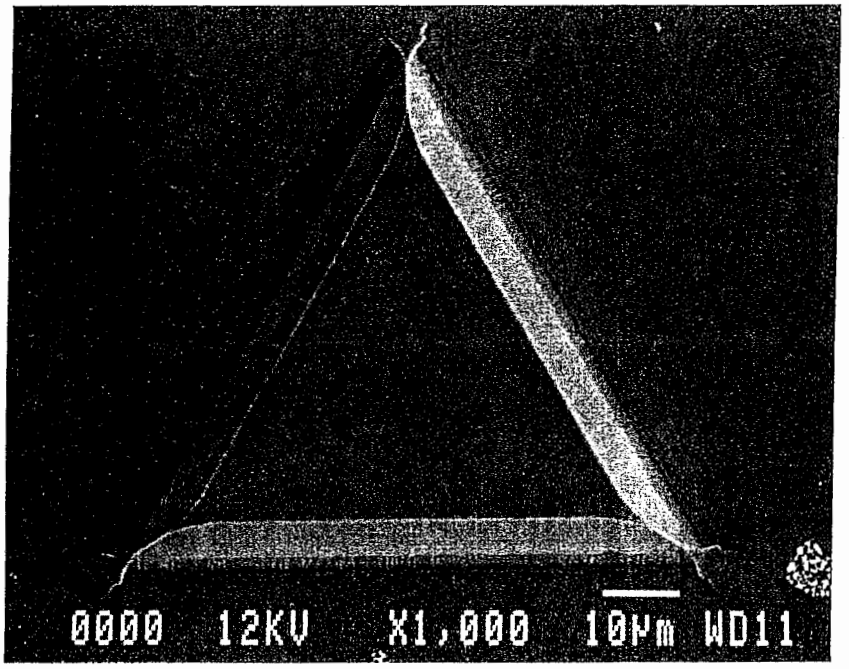

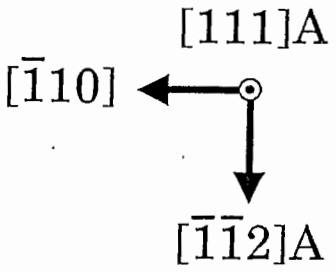

Figure 7 Top view of a 3.6 μm thick Si-doped GaAs layer grown on the (001) triangle with equivalent (113)A sidewalls.

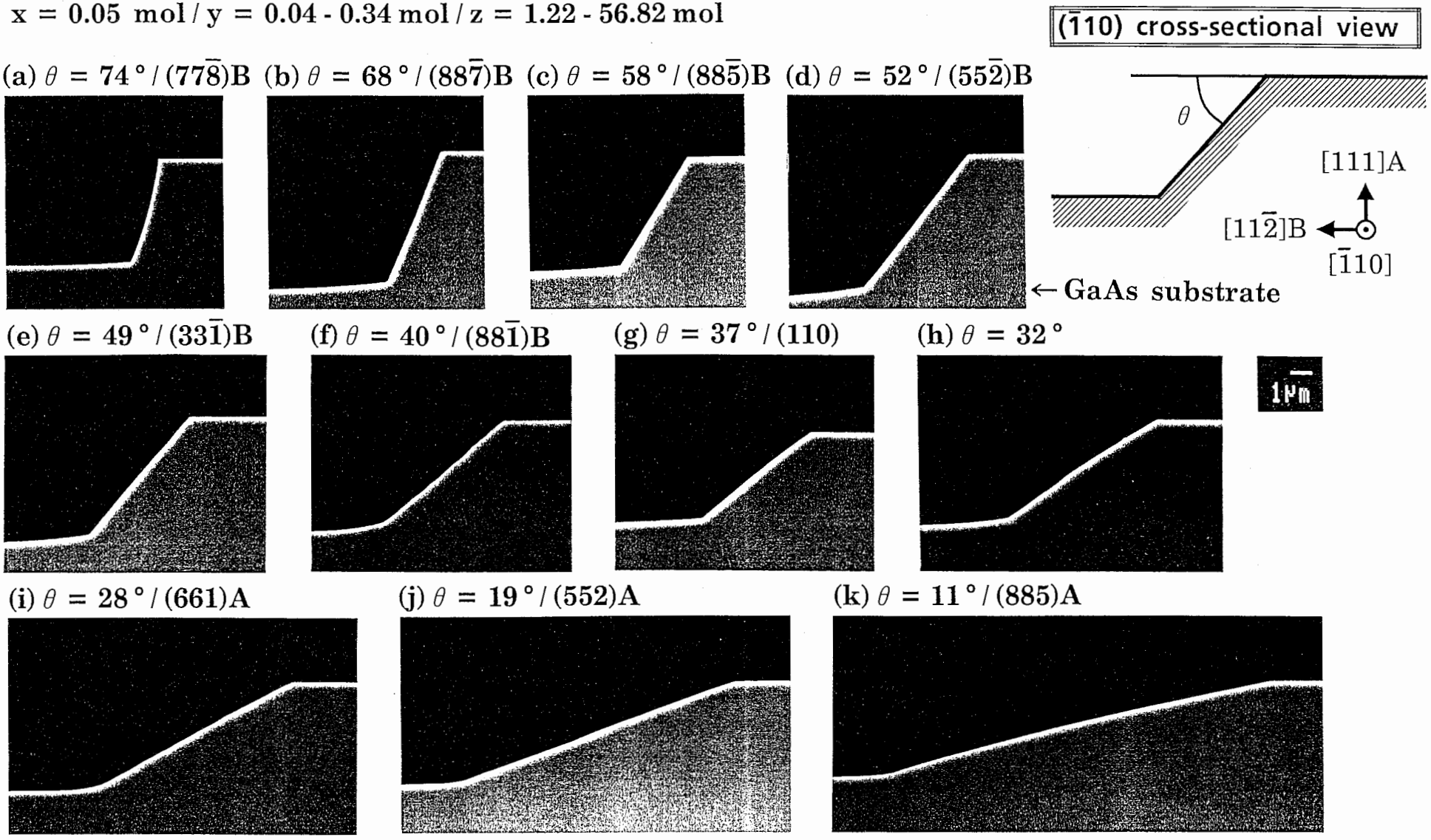

Figure 8 (1̄10) cross-sectional views of the as-etched profiles of the (110)-related sidewalls with various slopes.

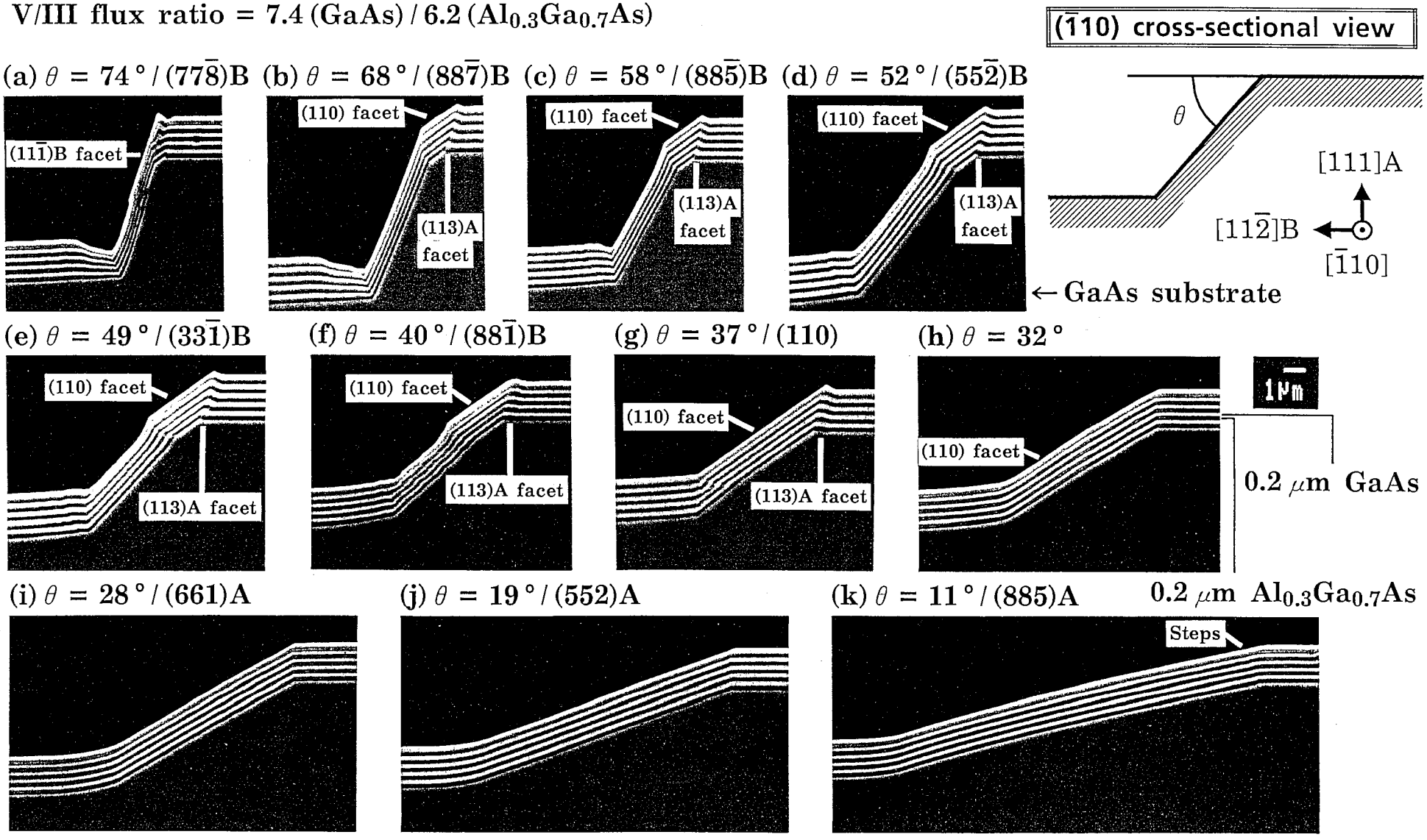

Figure 9 ($\bar{1}$10) cross-sectional views of the after-growth profiles of the (110)-related sidewalls corresponding to Figure 8.

$(11\bar{1})$B / θ_f = 71 °

(a) θ = 74 ° / $(77\bar{8})$B

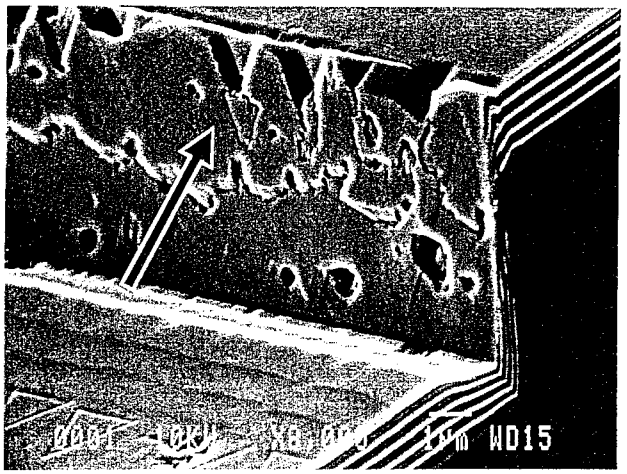

(b) θ = 68 ° / $(88\bar{7})$B

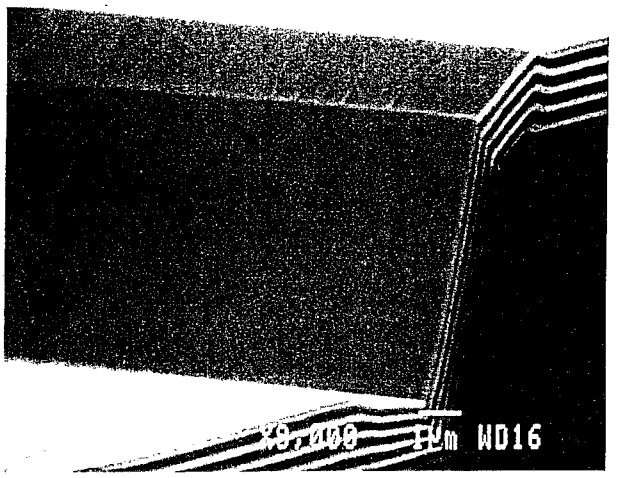

Figures 10 Bird's eye views of the growth behavior of the $(11\bar{1})$B facet (indicated by arrow) with respect to θ.

(110) / θ_f = 35°

(a) θ = 58° / (88$\bar{5}$)B

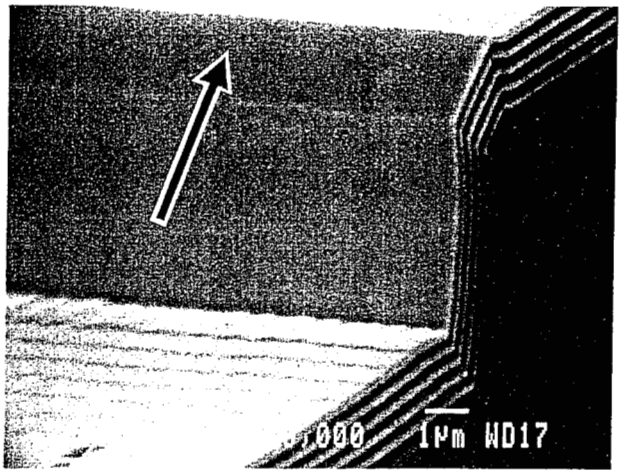

(b) θ = 49° / (33$\bar{1}$)B

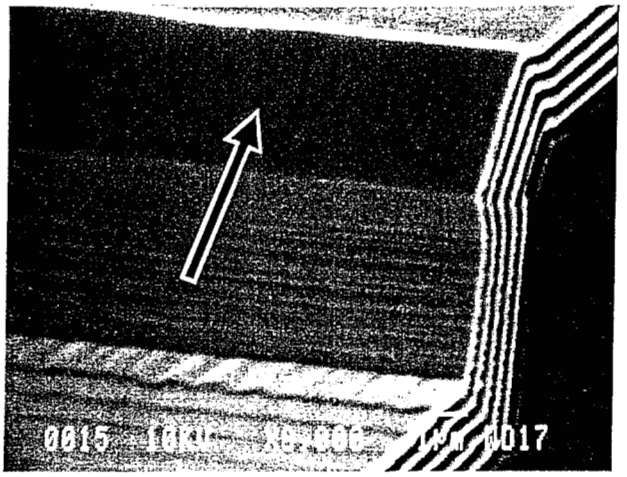

(c) θ = 40° / (88$\bar{1}$)B

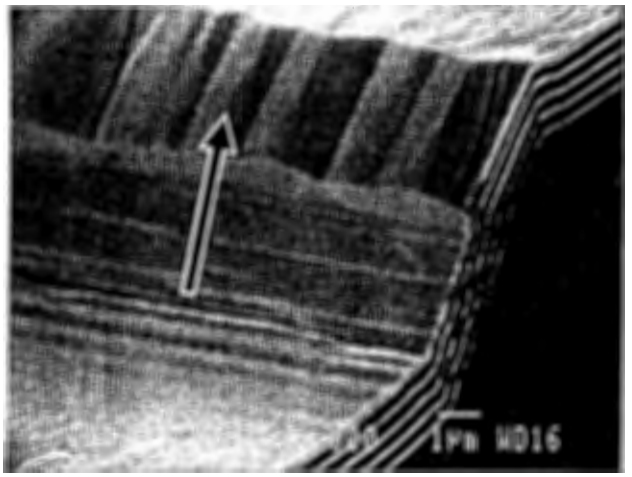

(d) θ = 37° / (110)

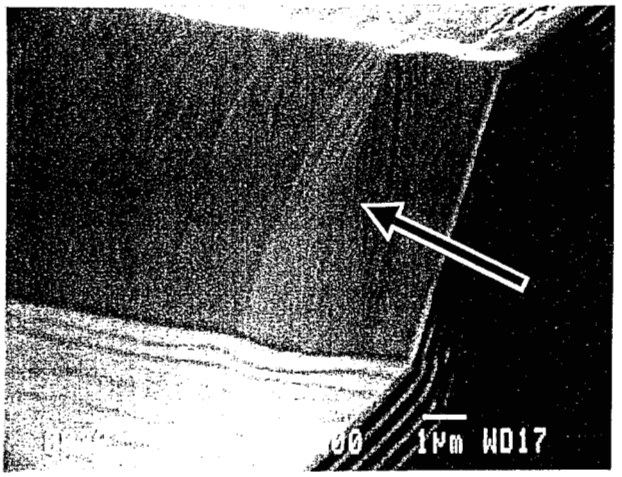

(e) θ = 32°

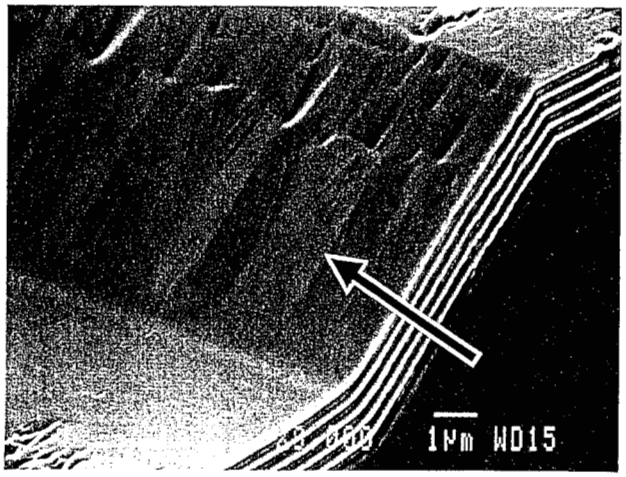

(f) θ = 28° / (661)A

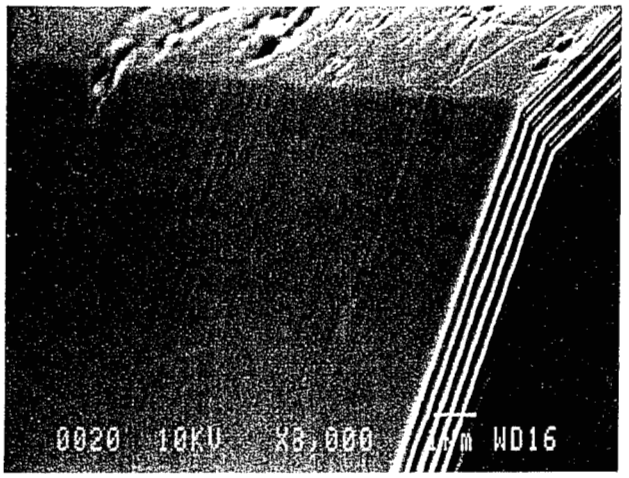

Figures 11 Bird's eye views of the growth behavior of the (110) facet (indicated by arrow) with respect to θ.

(a) θ = 40 °/(88$\bar{1}$)B

(b) θ = 32 °

"(110) triangle"

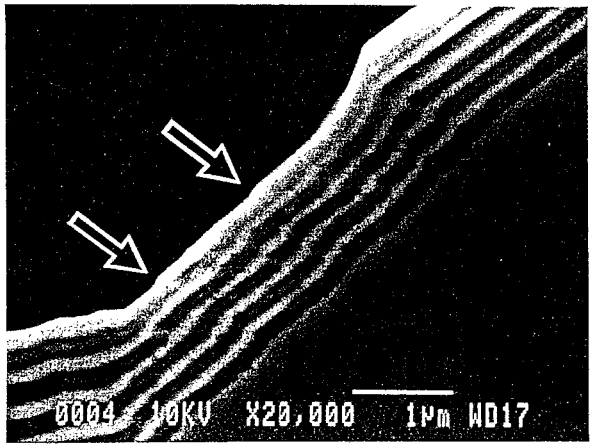

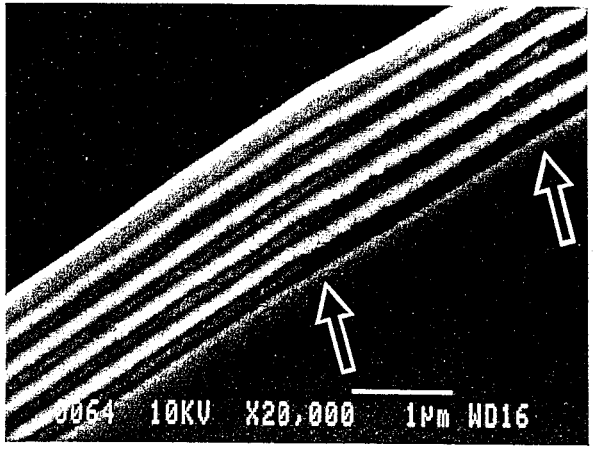

(c) θ = 41 °/(116)A

(d) θ = 36 °/(114)A

"(001) triangle"

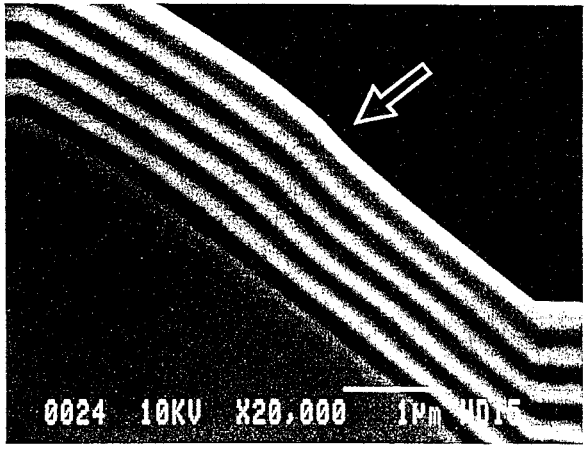

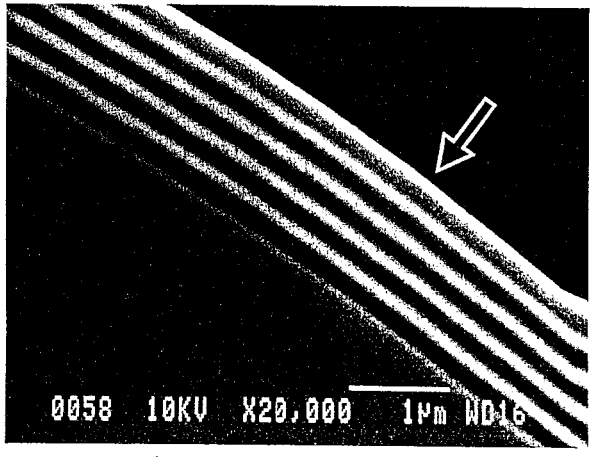

Figures 12 Magnified ($\bar{1}$10) cross-sectional views of (a) and (b) the (110)-related sidewalls with slopes around the facet angle of the (110) facet and (c) and (d) the (001)-related sidewalls with slopes around the facet angle of the (114)A facet.

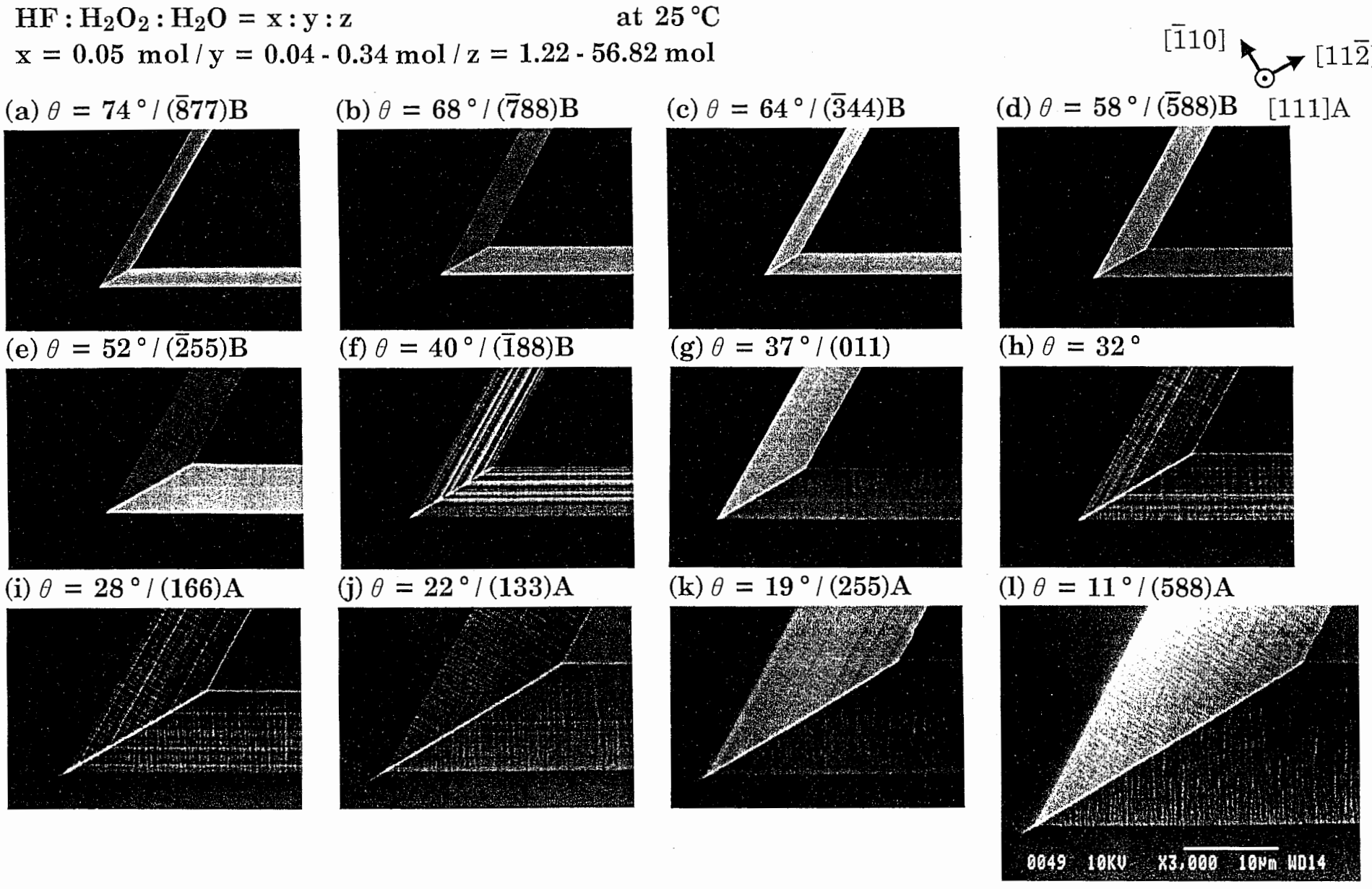

Figure 13 Top views of the as-etched profiles of the corners of the (110) triangles with various sidewall slopes.

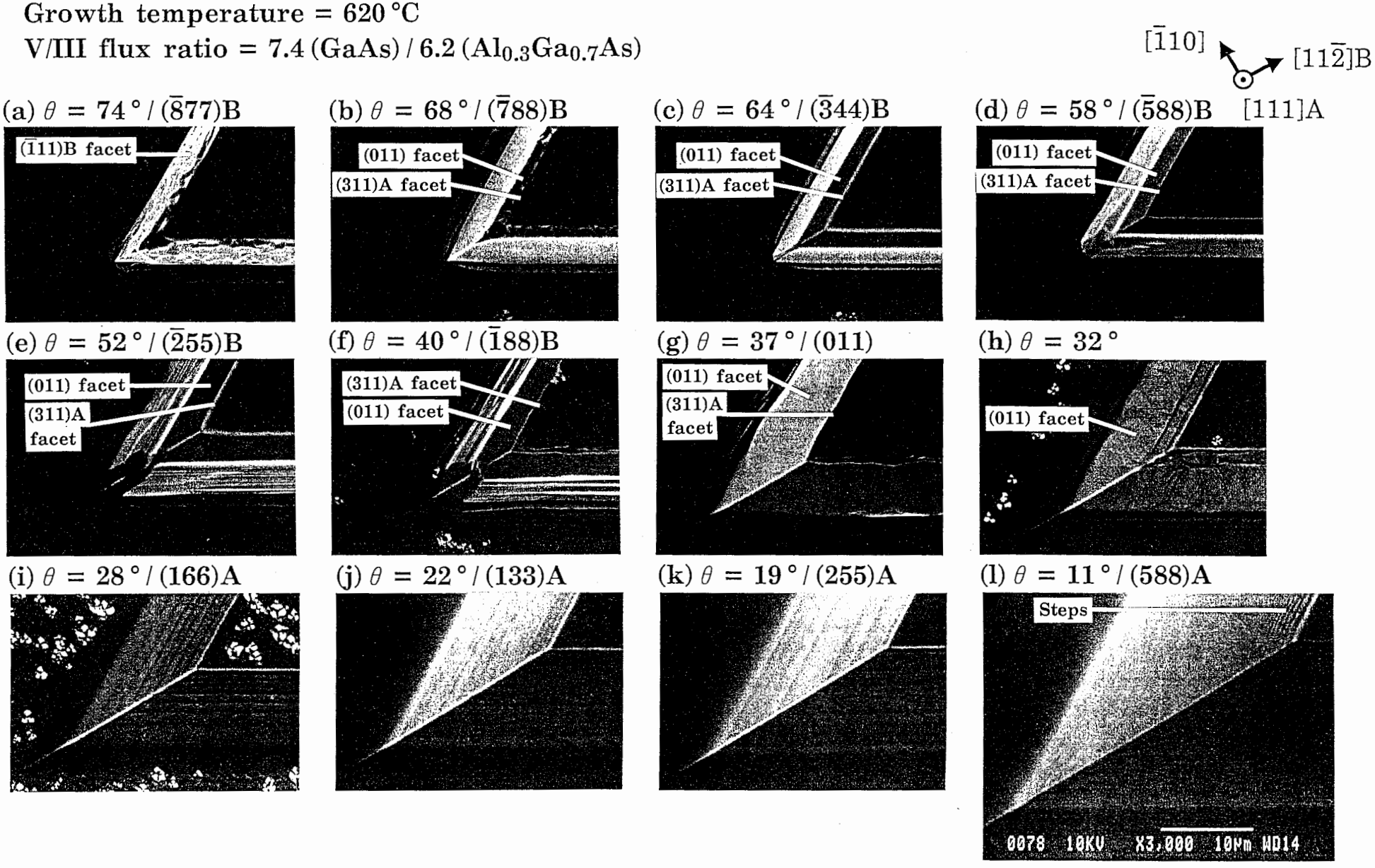

Figure 14 Top views of the after-growth profiles of the corners of the (110) triangles corresponding to Figure 13.

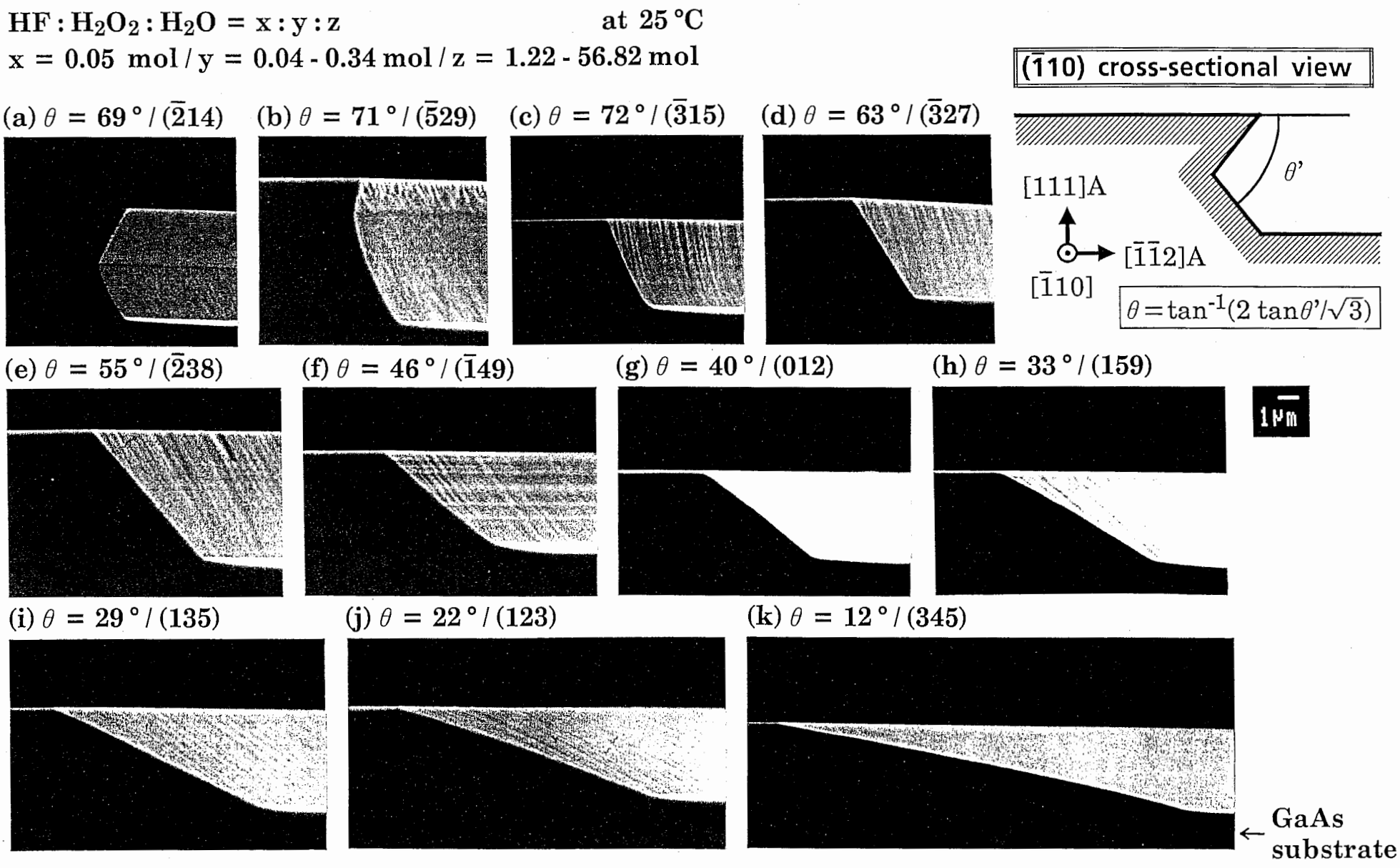

Figure 15 (1̄10) cross-sectional views of the as-etched profiles of the (201)-related sidewalls with various slopes.

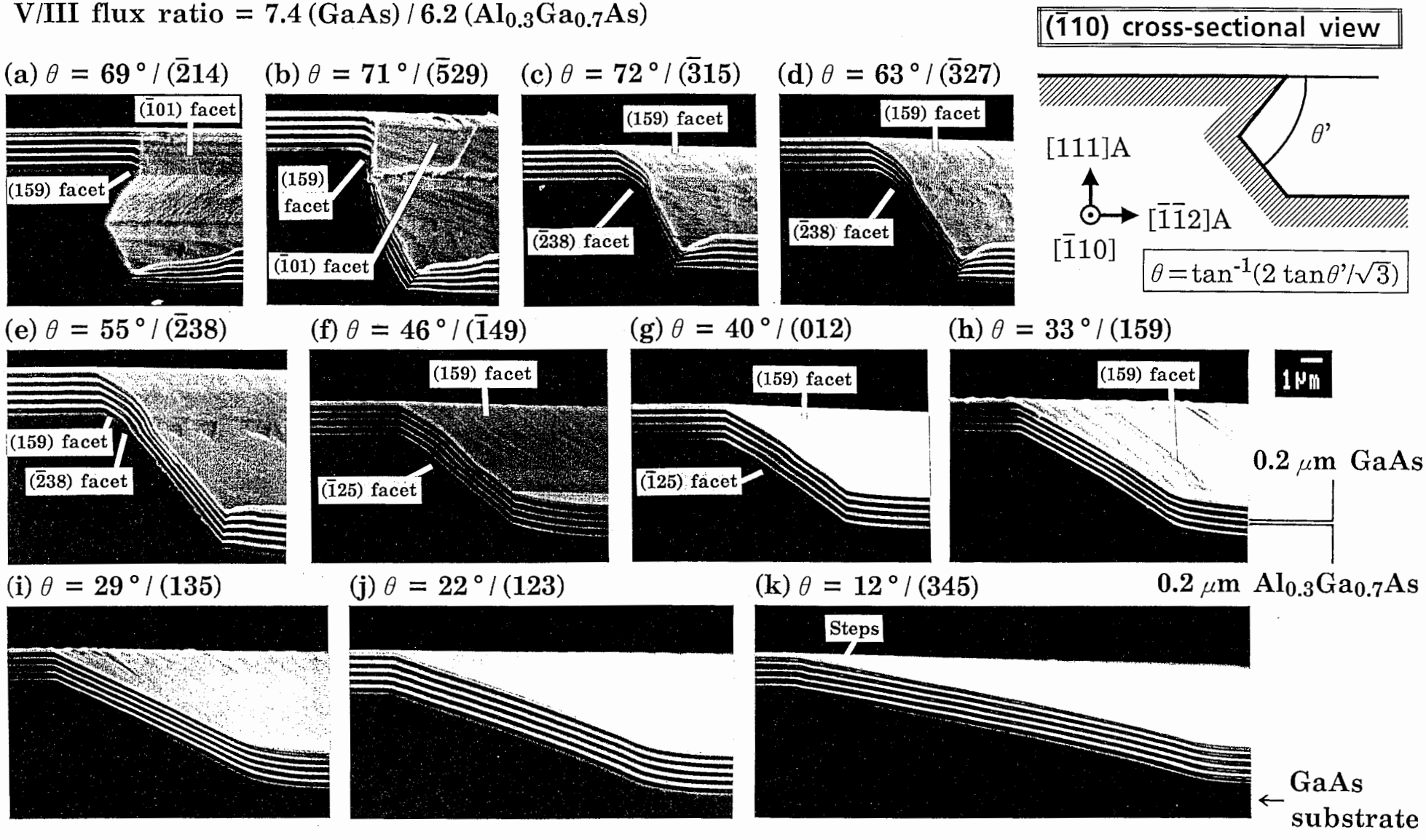

Figure 16 (1̄10) cross-sectional views of the after-growth profiles of the (201)-related sidewalls corresponding to Figure 15.

$(\bar{1}01)$ / $\theta_f = 90°$

(a) $\theta = 69°$ / $(\bar{2}14)$

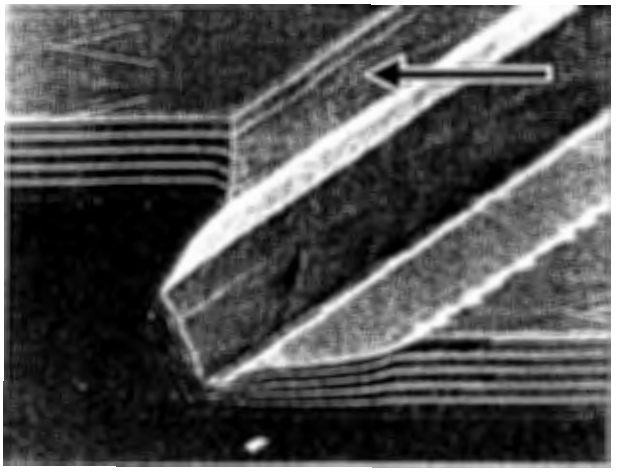

(b) $\theta = 71°$ / $(\bar{5}29)$

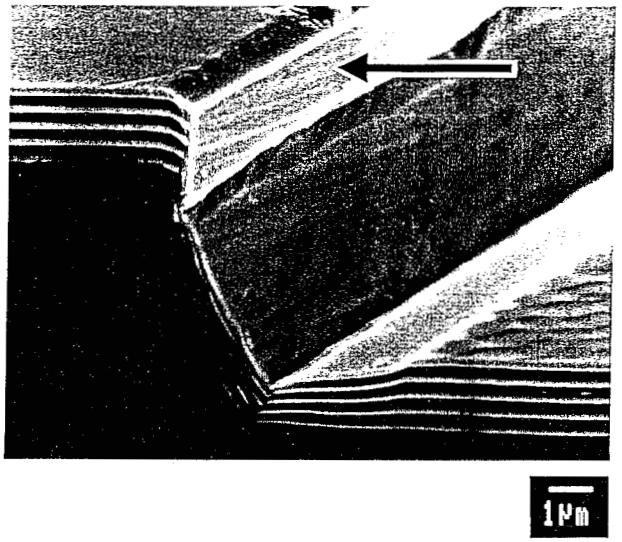

(c) $\theta = 72°$ / $(\bar{3}15)$

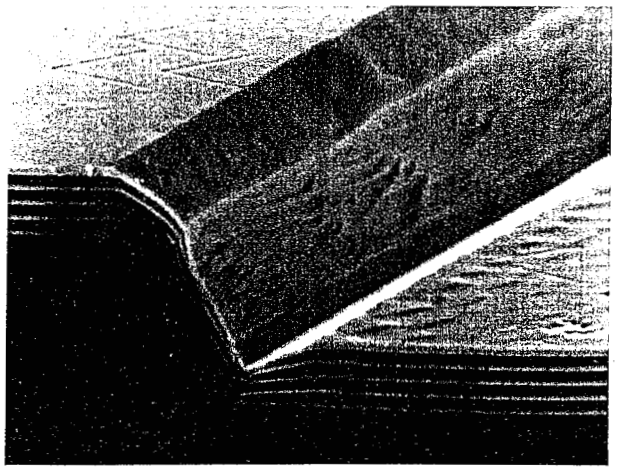

Figure 17 Bird's eye views of the growth behavior of the $(\bar{1}01)$ facet (indicated by arrow) with respect to θ.

(159) / θ_f = 34 °

(a) θ = 72 ° / ($\bar{3}$15)

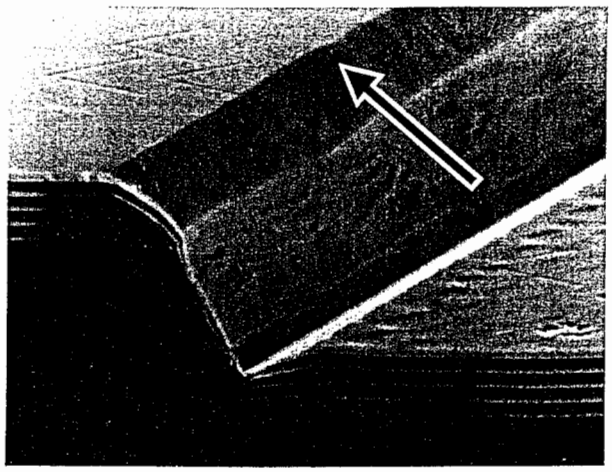

(b) θ = 55 ° / ($\bar{2}$38)

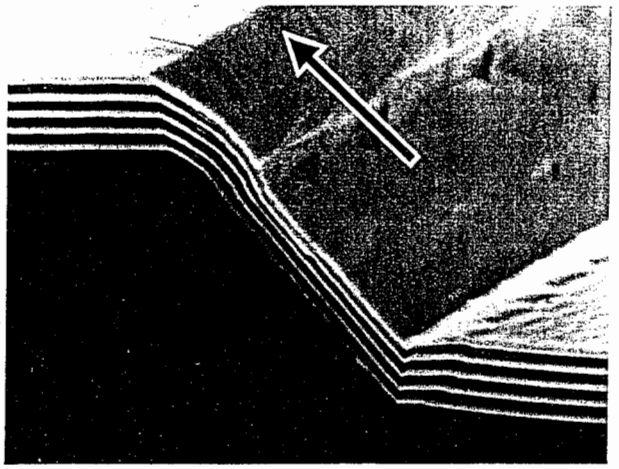

(c) θ = 46 ° / ($\bar{1}$49)

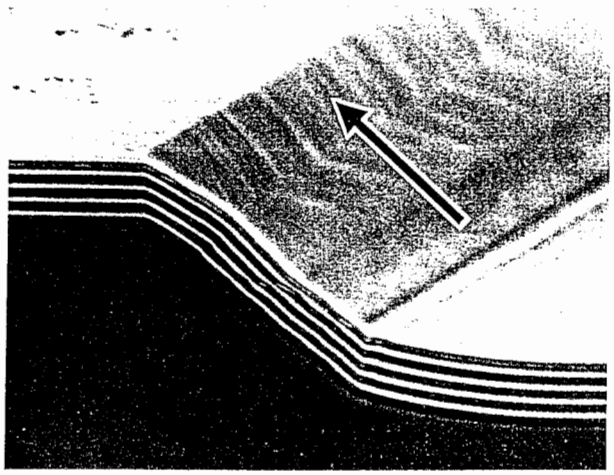

(d) θ = 40 ° / (012)

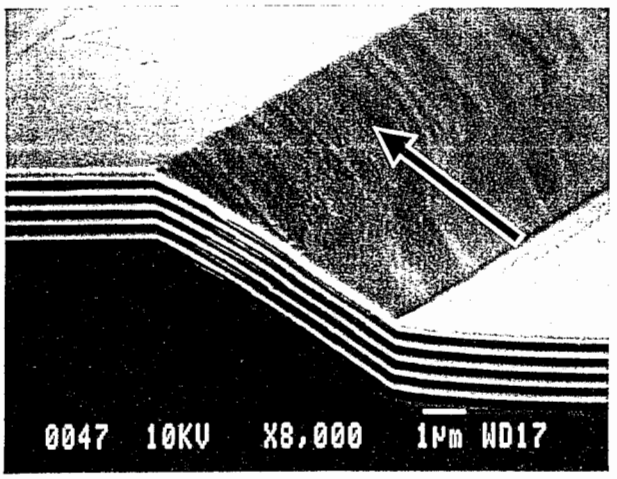

(e) θ = 33 ° / (159)

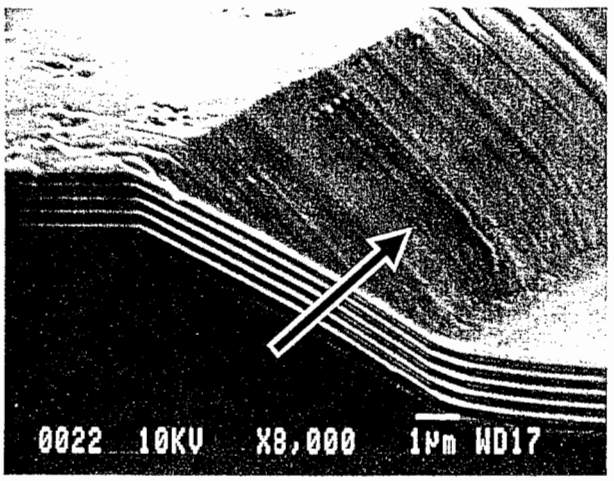

(f) θ = 29 ° / (135)

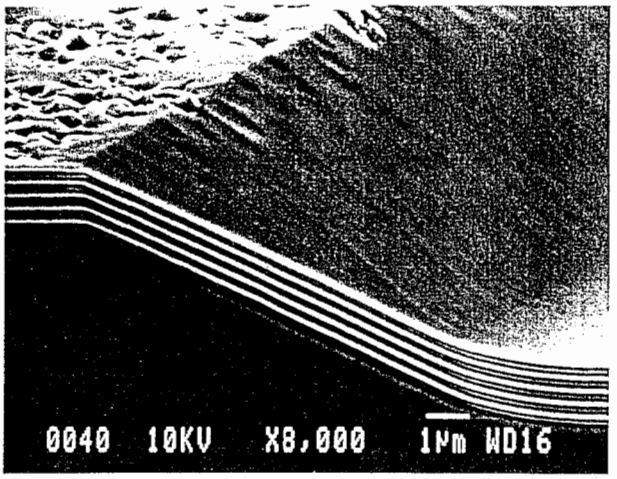

Figure 18 Bird's eye views of the growth behavior of the (159) facet (indicated by arrow) with respect to θ.

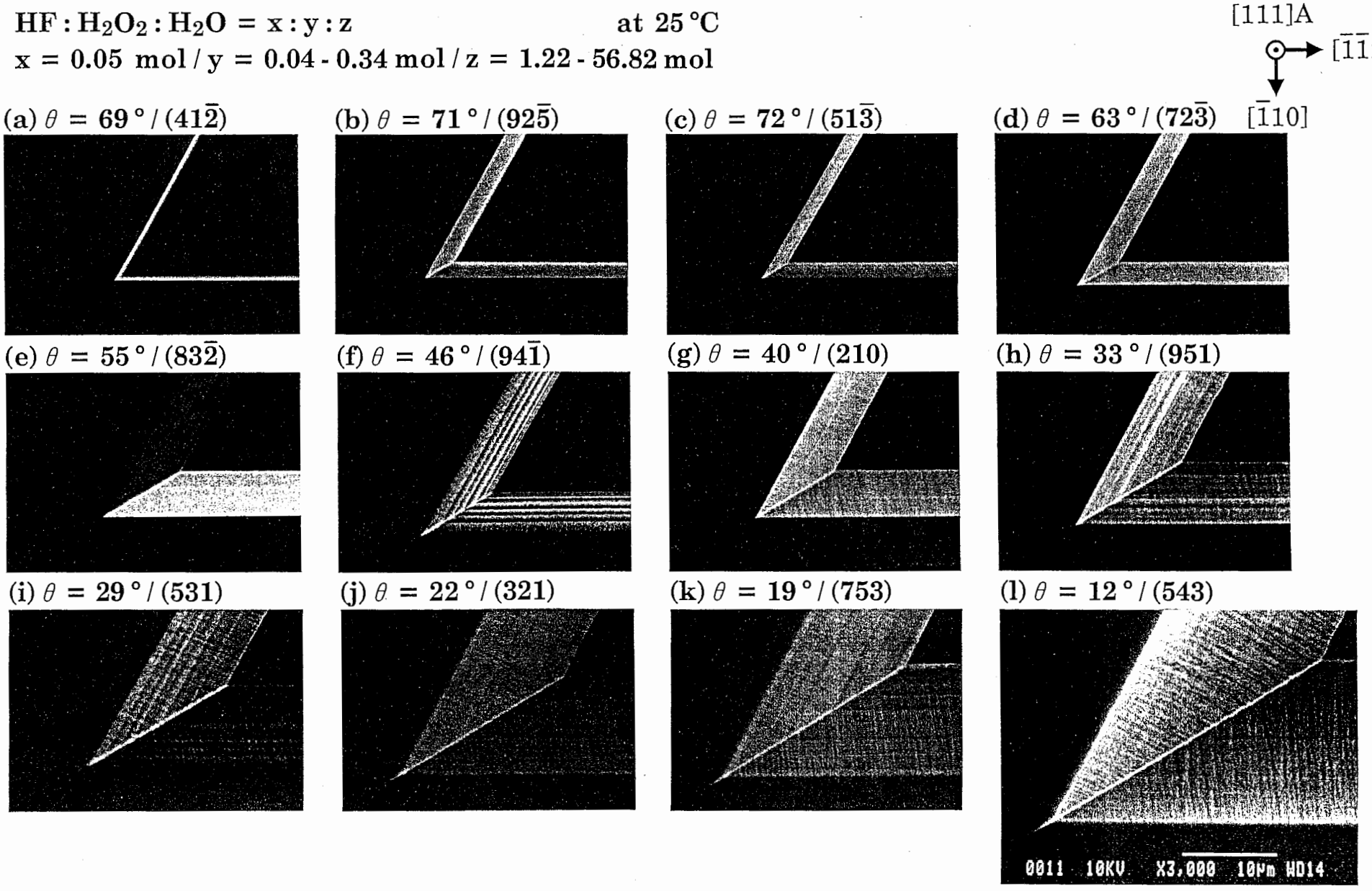

Figure 19 Top views of the as-etched profiles of the corners of the (021) triangles with various sidewall slopes.

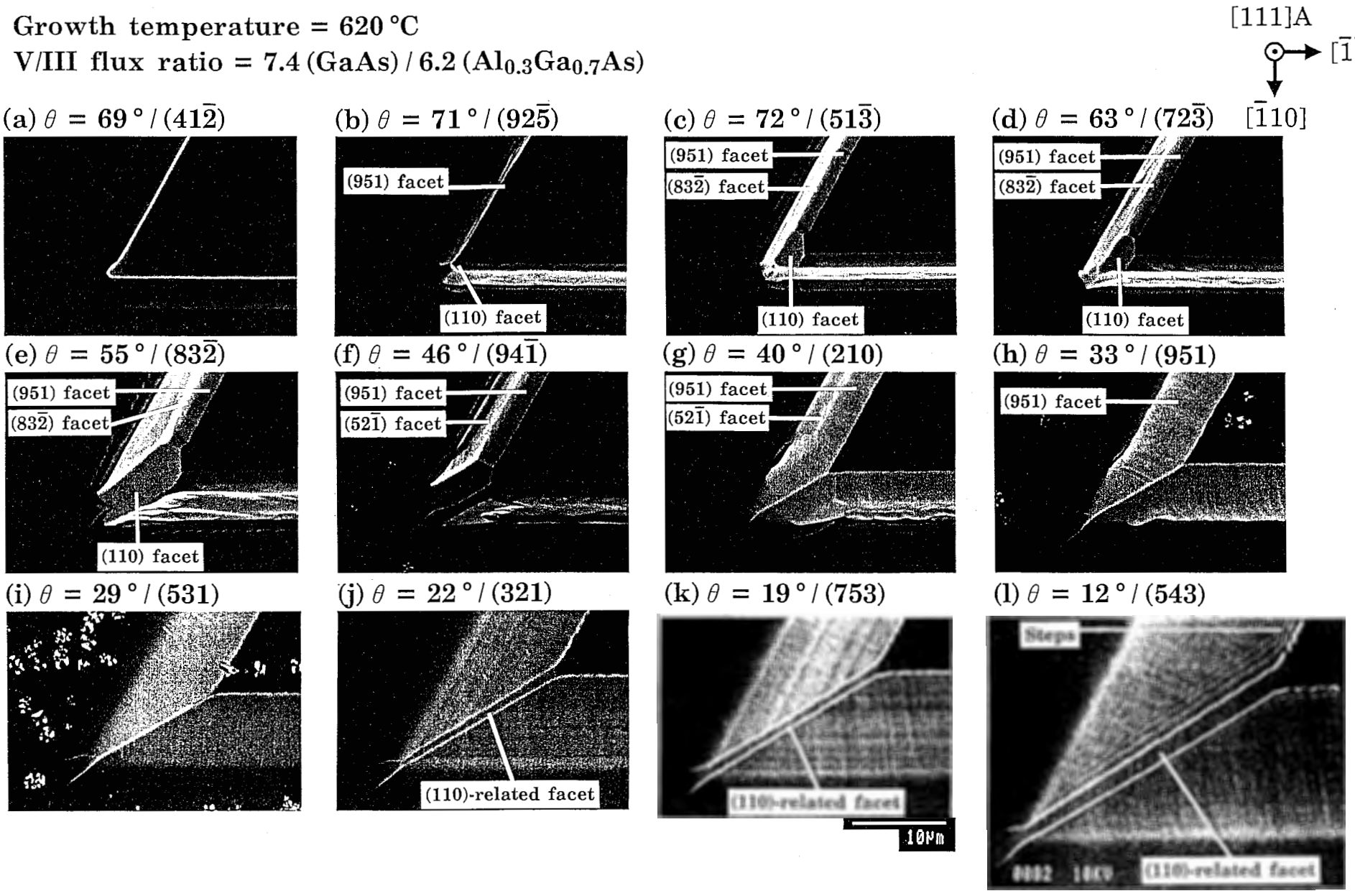

Figure 20 Top views of the after-growth profiles of the corners of the (021) triangles corresponding to Figure 19.

Growth temperature = 620 °C

(a) V/III flux ratio = 5.7

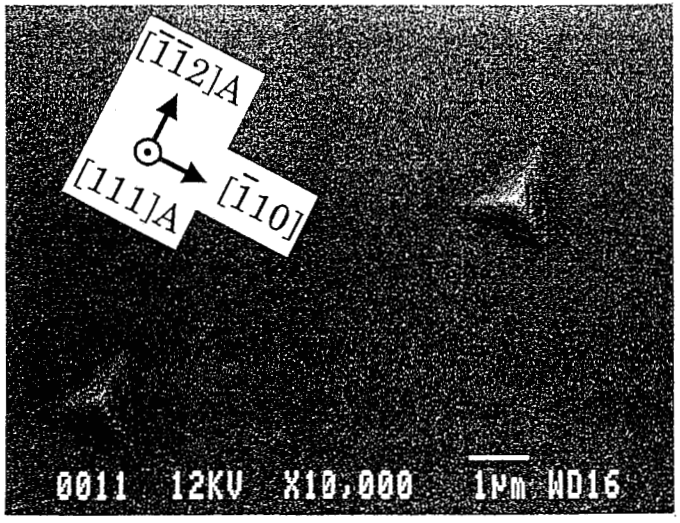

(b) V/III flux ratio = 7.6

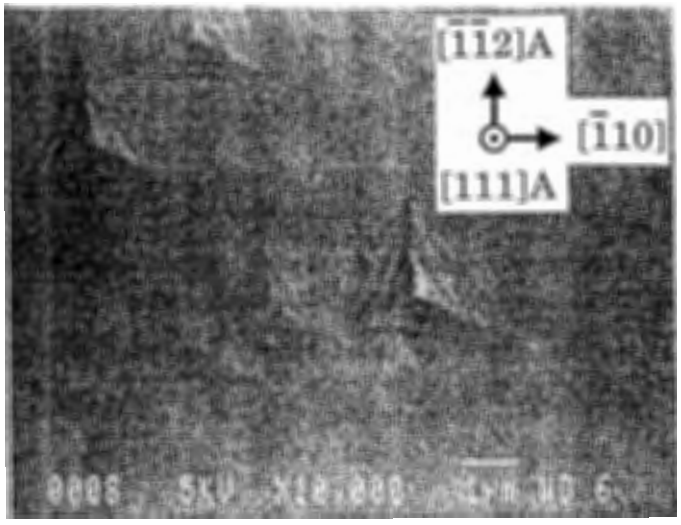

Figure 21 Pyramidal microstructures with (110)-related facets frequently observed on GaAs and AlGaAs layers grown on exact (111)A substrates.

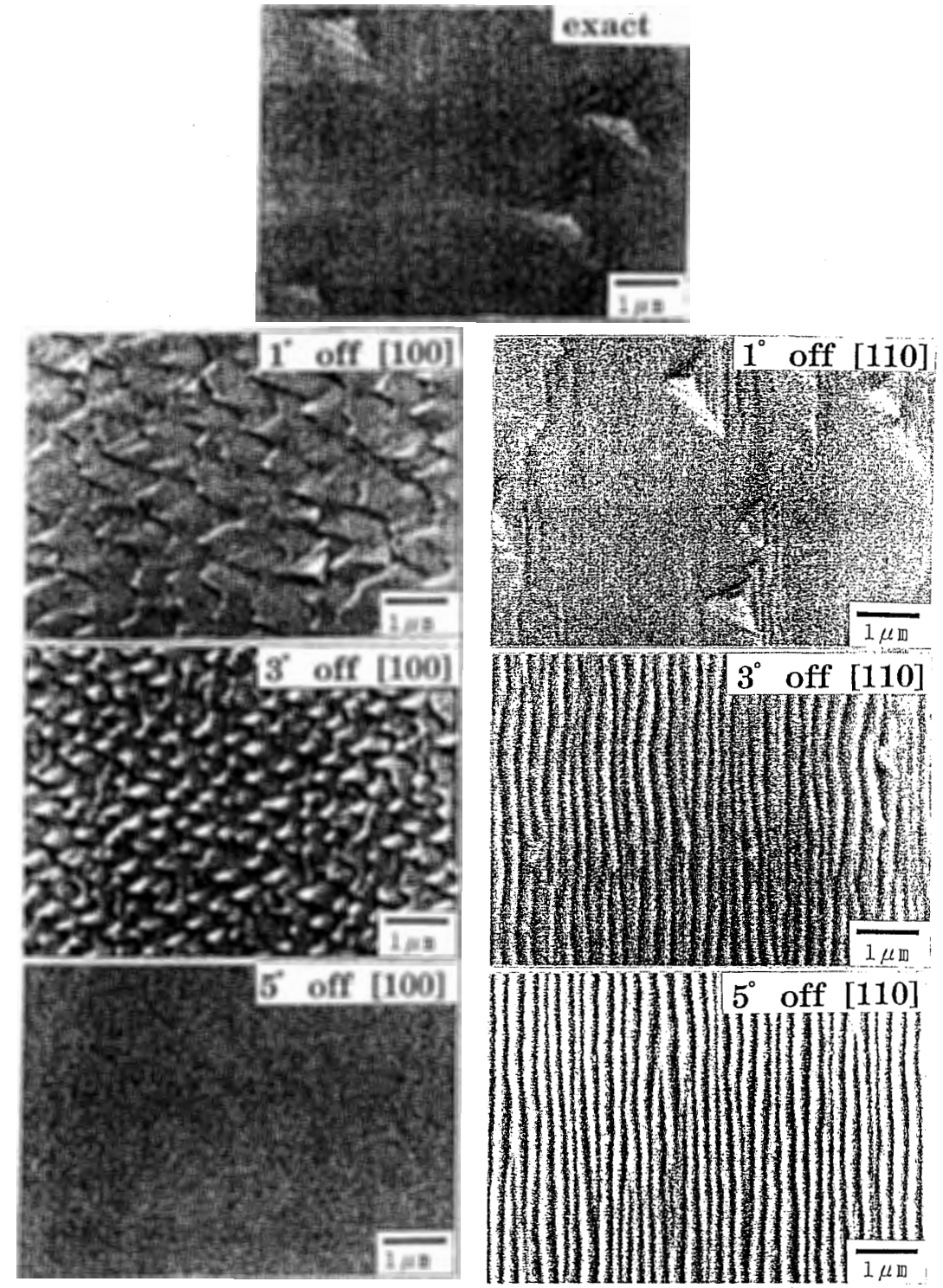

Figure 22 (110)-related step structures on GaAs and AlGaAs layers grown on misoriented (111)A substrates.

Misorientation = 3 ° towards the [001] direction

(a) "(110) triangle" : θ = 28 ° / (661)A

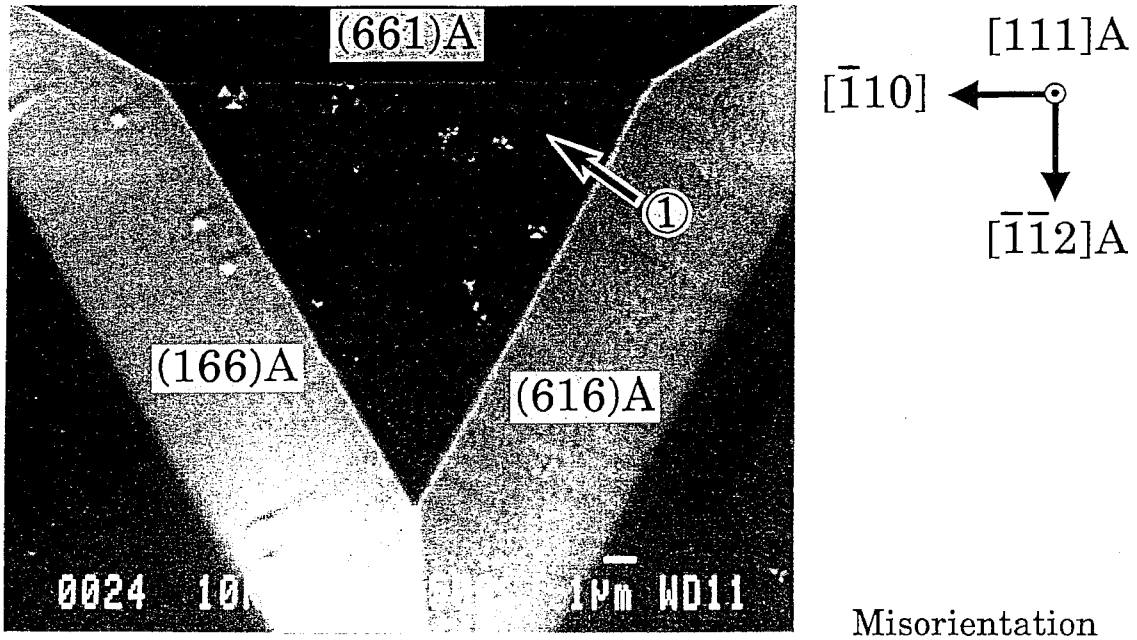

(b) "(001) triangle" : θ = 30 ° / (113)A

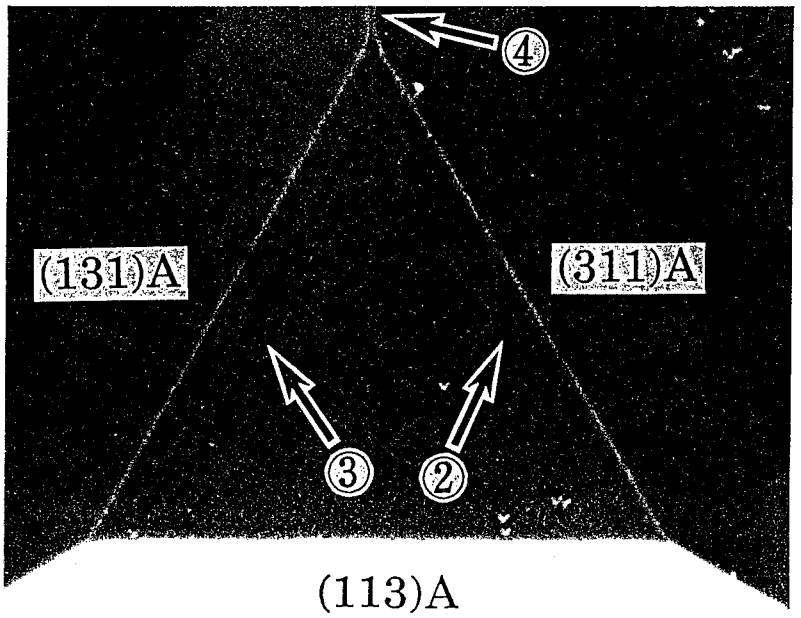

Figure 23 1μm thick Si-doped GaAs layers grown on (a) a (110) triangle and (b) a (001) triangle on a (111)A substrate misoriented by 3 ° towards the [001] direction.

Substrate	Sidewall slope	Extra facet on sidewall		Extra facet on corner	
(111)A	(001) triangle	Slope	Orientation	Slope	Orientation
	≧80°	80°	($\bar{1}\bar{1}$3)A	No facets	
		55°	(001)		
		33°	(114)A		
	80°～55°	55°	(001)	35°	(110)
		33°	(114)A		
	55°～33°	33°	(114)A	No facets	
	33°～29°	No facets		No facets	
	29°～16°	No facets		≦16°	(221)A etc.
	<16°	16°	(447)A		
	(110) triangle	Slope	Orientation	Slope	Orientation
	≧71°	71°	(11$\bar{1}$)B	No facets	
		35°	(110)		
	71°～55°	35°	(110)	No facets	
		30°	(113)A		
	55°～39°	35°	(110)	?	?
		30°	(113)A		
	39°～35°	35°	(110)	No facets	
		30°	(113)A		
	35°～30°	35°	(110)	No facets	
	30°～16°	No facets		No facets	
	<16°	16°	(221)A	No facets	
	(201) triangle	Slope	Orientation	Slope	Orientation
	Around 70° with inverted mesa	90°	($\bar{1}$01)	No facets	
		34°	(159)		
	72°～55°	56°	($\bar{2}$38)	35°	(110)
		34°	(159)		
	55°～51°	49°	($\bar{1}$25)	35°	(110)
		34°	(159)		
	51°～33°	49°	($\bar{1}$25)	No facets	
		34°	(159)		
	33°～26°	No facets		No facets	
	26°～17°	No facets		≦16°	(221)A etc.
	<17°	17°	(5 8 11)		

Table 1 Summary of facet generation behavior during MBE on GaAs (111)A patterned substrates.